Journal of Photochemistry, 24 (1984) 133 - 199

PICOSECOND AND NANOSECOND KINETIC SPECTROSCOPIC INVESTIGATIONS OF THE RELAXATION AND THE SOLUTE–SOLVENT REACTION OF ELECTRONICALLY EXCITED 3,5-DINITROANISOLE

C. A. G. O. VARMA, F. L. PLANTENGA, A. H. HUIZER, J. P. ZWART, Ph. BERGWERF and J. P. M. VAN DER PLOEG

Department of Chemistry, Gorlaeus Laboratories, State University, P.O. Box 9502, 2300 RA Leiden (The Netherlands)

(Received June 22, 1983)

Summary

We investigated the relaxation of electronically excited nitro aromatic compounds, in particular 3,5-dinitroanisole (3,5-DINA), by means of picosecond and nanosecond laser kinetic spectroscopy. Complete neglect of differential overlap/spectroscopic–configuration interaction calculations were performed to characterize their excited states. The gas phase UV spectrum of 3,5-DINA and the electron spin resonance spectrum of the anion serve the same purpose. It is shown by means of IR spectroscopy that 3,5-DINA in its ground state does not form hydrogen bonds. The envelope of the first absorption band of 3,5-DINA in liquid solutions covers a weak $n\pi^*$ and a strong $\pi\pi^*$ transition. In non-hydrogen-bonding solvents, excitation in this band populates a primary excited state S_i which decays within 10 ps to S_0 and to T_0. The state T_0 (in CH_3CN) is converted within 780 ps to S_0. In hydrogen bonding solvents the decay is quite different. The conversion $T_0 \rightarrow S_0$ and probably $S_i \rightarrow S_0$ is much slower, while the intersystem crossing $S_i \rightarrow T_0$ remains very fast. We conclude that in aprotic solvents both S_i and T_0 are $n\pi^*$ states in which the excitation is localized on the NO_2 groups, which are consequently distorted to a large extent relative to the ground state. The distortion is thought to cause strong phonon coupling in the radiationless transitions $S_i \rightarrow S_0$ and $T_0 \rightarrow S_0$. Local vibrations in the NO_2 group, which modulate the overlap of lone pair orbitals on adjacent oxygen atoms, are efficient promoting modes in the radiationless decay and they make the rate constant much larger than in other cases involving local excitation of small chromophores, *e.g.* ketones. The primary state populated by excitation with our pulsed lasers is a $\pi\pi^*$ charge transfer state. When 3,5-DINA is brought into this state in hydrogen bonding solvents, it forms a (single) hydrogen bond before any other type of relaxation. Thus S_i and T_0 are both hydrogen-bonded delocalized $\pi\pi^*$ states. The known efficient bimolecular photo-induced reactions of 3,5-DINA involve the formation of the hydrogen bond as the first step. A reinterpretation is given of the variation in the

0047-2670/84/$3.00

triplet lifetime of 3,5-DINA over three orders of magnitude with solvent composition. The thermal dissociation of the hydrogen bond to the NO_2 group is the rate-determining step in the decay of 3,5-DINA in hydrogen bonding solvents. Both the activation energy and the activation entropy of this reaction depend on the solvent structure.

1. Introduction

Surprising modifications in chemical and spectroscopic behaviour of aromatic molecules arising from the introduction of NO_2 groups as substituents have challenged many chemists to find an explanation for the influence of these substituents on the molecular properties. In their search they have focused attention mainly on relations between the molecular electronic structure of the isolated molecule on the one hand and reactions on the other hand [1 - 4].

The origin of the investigations reported here was a dilemma in the understanding of photo-induced bimolecular reactions of nitro aromatic compounds in solution. Although many of the nitro aromatic compounds exhibit absolutely no fluorescence or phosphorescence after electronic excitation, not even in glassy matrices, the excited species may be transformed efficiently in a bimolecular chemical reaction. Absence of emissions suggests that very fast electronic relaxation deactivates the excited states [5]. These two aspects are particularly clear in the photo-induced reaction of 3,5-dinitroanisole (3,5-DINA) with OH^- where the quantum yield of the product 3,5-dinitrophenolate may be as high as 0.27 when the concentration of OH^- is only 8.0×10^{-4} M [6]. From this it follows that the reacting state should have a lifetime of the order of 10^{-6} s. In this case we have established that the reacting state is a $\pi\pi^{**}$ triplet state which has a lifetime of several microseconds in aqueous solution at room temperature. Such a relatively long-lived triplet state is expected to phosphoresce at low temperatures but no emission is observed.

The photohydrolysis of 3,5-DINA is a representative example of a large number of interesting photo-induced reactions of nitro aromatics which have been reported [7]. The majority of these involve a nucleophilic substitution of an ether or an ester group. In interpreting the results attempts have been made to correlate the product yields to an enhancement in the reactivity of ring carbon atoms in the *meta* position relative to the NO_2 groups. However, it should be realized that such correlations can only be meaningful if there are no intermediate chemical transformations before the attack by the nucleophile. For the reaction of 3,5-DINA with OH^- reaction intermediates have been discovered recently with the aid of time-resolved spectroscopic techniques [6]. In the course of this reaction a rather complex sequence of parallel reactions was observed in some of which the solvent proved to be

involved, directly as a reagent or indirectly by influencing branching ratios of parallel reactions.

The aim of the present work is to shed light on the relaxation processes that take place after electronic excitation of nitroanisoles, before photosubstitution of the OCH_3 group. The processes have been studied in several solvents to trace solvent effects on the relaxation processes. In Section 3 we present a study on a picosecond time scale of the kinetics involved in the population and decay of excited states of 3,5-DINA, 3-nitroanisole (3-NA), 4-*tert*-butyl-3,5-dinitroanisole (B-DINA) and the perdeutero isomer of 3,5-DINA, initiated by excitation with a laser pulse of about 10 ps duration. The results offer insight into the very fast decay of the primary excited states S_i of the nitroanisoles and how this is affected by hydrogen bonding and solvent polarity. From the experiments we are able to derive rate constants for the $S_i \rightarrow T_0$, $S_i \rightarrow S_0$ and $T_0 \rightarrow S_0$ processes. In particular we have tried to elucidate the mechanism of the decay by studying the effects of deuteration, steric hindrance and solvent polarity on the kinetics of the decay processes. Also the effects of low temperatures and solid matrices are investigated. By analysing the kinetics of triplet state formation in solvent mixtures of H_2O and CH_3CN with various H_2O concentrations an insight could be obtained into the hydrogen bonding reaction between the excited 3,5-DINA molecules and H_2O molecules.

Predissociation of the C—NO_2 bond has previously been held responsible for the absence of any fluorescence from excited nitro aromatic compounds which have their first excited singlet state more than 20 000 cm^{-1} above the ground state [8 - 10]. For 3,5-DINA predissociation as a major decay channel seems to be ruled out because of the absence of photodissociation products and because triplet state reactions give high yields of substitution products with the C—NO_2 bond preserved [7]. This leads to the conclusion that the very fast $S_i \rightarrow S_0$ and $T_0 \rightarrow S_0$ decay processes are nearly pure intramolecular processes. Some ideas about the mechanism underlying the fast decay are given in Section 3.

The interpretation of the observed kinetics rests on a knowledge of the electronic energy level scheme shown in Fig. 1 and of some properties of the excited states of the nitroanisoles. The energy level scheme is derived from UV spectra, photoelectron spectra and complete neglect of differential overlap/spectroscopic-configuration interaction (CNDO/S–CI) calculations presented in Section 4.1. It shows that the nitroanisoles have closely spaced $n\pi_1^*$ and $\pi\pi_1^*$ states, in both the singlet and the triplet manifold. These $n\pi_1^*$ and $\pi\pi_1^*$ states are thought to have widely differing properties with respect to hydrogen bonding and radiationless decay. It will be shown that both S_i and T_0 of the nitroanisoles in non-polar solutions have a very efficient radiationless decay channel to the ground state and that this fast decay can be associated with the $n\pi_1^*$ states. The rate of this decay is reduced appreciably when the excited molecule forms a hydrogen bond with an H_2O or alcohol molecule. Owing to hydrogen bonding the $^3\pi\pi_1^*$ state becomes the lowest triplet state in 3,5-DINA and this state has a much lower rate of

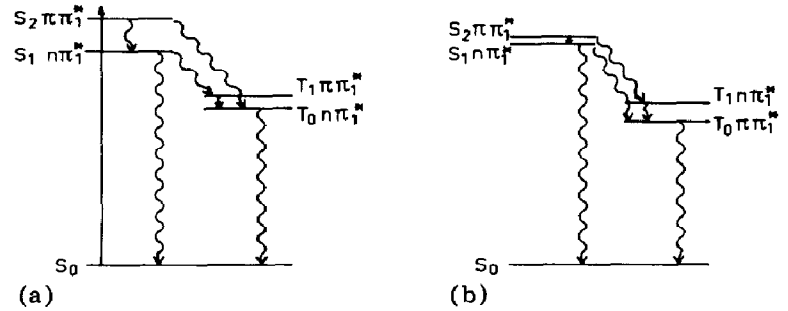

Fig. 1. Energy level scheme of 3,5-DINA to be used in the explanation of the observed relaxation kinetics. π_1^* is the lowest unoccupied π orbital relative to the occupation in S_0. Solutions in non-hydrogen-bonding and in hydrogen bonding solvents are given in (a) and (b) respectively.

decay than the $^3n\pi_1^*$ state. The hydrogen bonding reaction takes place between the $^1\pi\pi_1^*$ charge transfer state and an H_2O or alcohol molecule. This reaction can be described as a first-order reaction in the concentration of H_2O.

Details of the nature of the hydrogen bond(s) formed in the excited state could be derived from an electron spin resonance (ESR) study of the negative ion of 3,5-DINA in aqueous solution, which reveals that only a single NO_2 group in the anion forms a strong hydrogen bond. This is discussed in Section 4.2. As a consequence of the hydrogen bond the extra electron in the anion becomes almost localized on that particular NO_2 group. Since the $\pi\pi_1^*$ charge transfer state is very similar to the ground state of the anion, we expect that also in the excited state only one NO_2 group may form a hydrogen bond, which will lead to a localization of negative charge on that NO_2 group. CNDO/S–CI calculations show that the π_1^* lowest unoccupied molecular orbital is highly localized on the NO_2 groups. A calculation on the supermolecule 3,5-DINA–H_2O indeed confirms the charge localization in the $\pi\pi_1^*$ excited state on one of the two NO_2 groups due to hydrogen bonding.

In an early stage of the investigation an optical absorption of 3,5-DINA in its lowest triplet state T_0 was found [11]. The observed lifetime τ of the triplet state showed a variation of more than three orders of magnitude as a function of solvent composition and temperature. At the time it was thought that rapid intersystem crossing to the ground state was predominantly determined by a strong dependence of the electronic wavefunctions on the torsional motions of the NO_2 group, which could modulate the delocalization of the π electrons over the phenyl ring and NO_2 groups. The remarkable variation in decay rate constant of T_0 with the concentration of H_2O in mixed aqueous solvents was thought to arise from variations in the size and structure of the H_2O clusters hydrogen bonded to the NO_2 groups, thus inhibiting the torsional motion of the NO_2 groups. A reinterpretation of this phenomenon is given in Section 4.3 on the basis of an investigation of the temperature dependence of the triplet decay.

2. Experimental details

The spectrometer used in our picosecond time-resolved spectroscopic investigations is shown in Fig. 2. An amplified single pulse selected from the train of pulses emerging from a mode-locked Nd^{3+} glass laser is sent along two beam directions. In one beam either the third or the fourth harmonic of the fundamental laser frequency is generated and then used to provide the primary excitation of the sample. In the other beam a spectral continuum is generated after a variable delay. After rejection of the fundamental frequency component, the bandwidth of the continuum is limited by an interference filter to 10 nm full width at half-maximum (FWHM). A beam splitter divides the continuum into a reference and a probing beam. The time delay between arrival of the excitation and the probing pulse at the sample is adjustable in the interval $0\ \text{ns} \leqslant \Delta t \leqslant 2\ \text{ns}$ with a precision of 0.06 ps. The probe, reference and excitation pulses are monitored by vacuum photodiodes which transmit their output signals to a 500 MHz transient digitizer. The digitized signals are stored in a computer memory and are used to calculate the pseudo-optical density $R(\Delta t)$ according to eqn. (8).

The peak of the excitation pulse arrives at the sample at time $t = 0$ and the pulse intensity $I_{ex}(t)$ is given by

$$I_{ex}(t) = \frac{A_{ex}}{\sigma(2\pi)^{1/2}} \exp\left(-\frac{t^2}{2\sigma^2}\right) \tag{1}$$

The intensity $I_p^{(0)}(t)$ of the unattenuated probe pulse, delayed by an amount Δt with respect to the excitation pulse, is given by

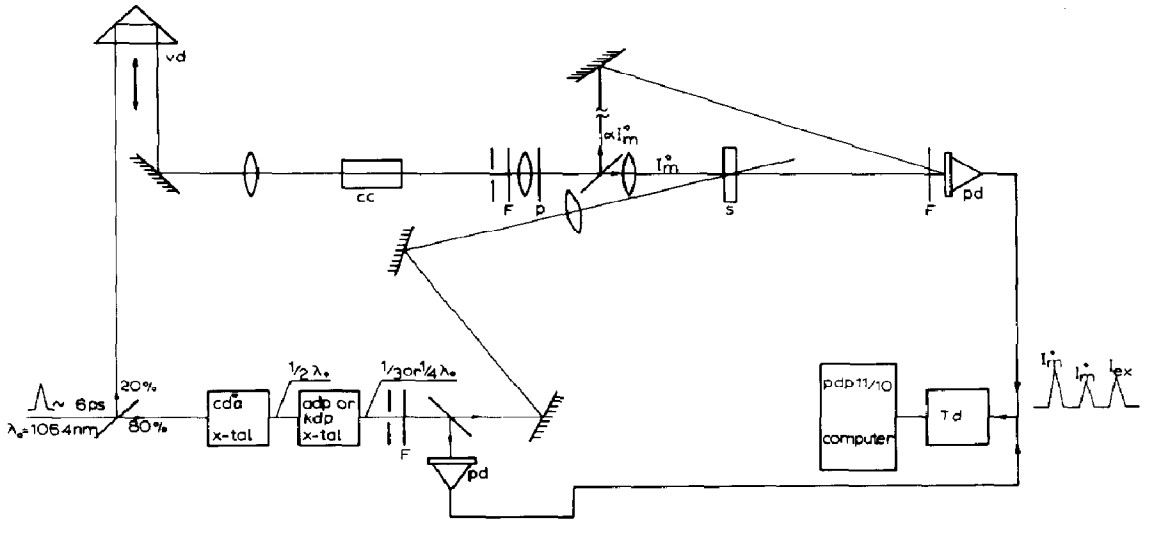

Fig. 2. Spectrometer for double-beam picosecond kinetic spectroscopy using an amplified single pulse from a mode-locked Nd^{3+} glass laser oscillator: cc, continuum cell; F, filter; p, polarizer; pd, photodiode; s, sample; vd, variable delay.

$$I_p^{(0)}(t) = \frac{A_p}{\sigma(2\pi)^{1/2}} \exp\left\{-\frac{(t-\Delta t)^2}{2\sigma^2}\right\} \tag{2}$$

In eqns. (1) and (2) the width of the pulse is represented by 2σ and the area under the pulse envelope is denoted by A_{ex} and A_p respectively. The intensity of the transmitted pulse follows from the Lambert–Beer law:

$$I_p(t) = I_p^{(0)}(t) \times 10^{-D(t)} \tag{3}$$

Here $D(t)$ is the transient optical density of the sample at time t. One photodiode determines the time integrals U_1 and U_2 of the transmitted and unattenuated probe pulse:

$$U_1(\Delta t) = \frac{A_p}{2} \int_{-\infty}^{+\infty} 10^{-D(t)} \exp\left\{-\frac{(t-\Delta t)^2}{2\sigma^2}\right\} dt \tag{4}$$

$$U_2 = \int_{-\infty}^{+\infty} I_p^{(0)}(t)\, dt \tag{5}$$

Another photodiode determines the time integral V of the excitation pulse:

$$V = \int_{-\infty}^{+\infty} I_{ex}(t)\, dt \tag{6}$$

The ratios

$$r = U_2/U_1 \tag{7a}$$

and

$$r' = U_2'/U_1' \tag{7b}$$

are determined. The prime refers to the circumstance in which the primary excitation beam does not enter the sample cell. The transient pseudo-optical density, normalized with respect to the primary excitation energy, is defined by

$$R(\Delta t) = \frac{\log_{10}(r'/r)}{V} \tag{8}$$

If the sample is transparent before the primary excitation, $R(\Delta t)$ is equal to the quantity $R_s(\Delta t)$ given by

$$R_s(\Delta t) = \frac{\log_{10}(U_2/U_1)}{V} \tag{9}$$

which is used in simulations of the time dependence of $R(\Delta t)$.

The width of the laser pulse, *i.e.* 2σ, may be determined from the profile of $R(\Delta t)$ for a transient absorption which follows the preparation pulse instantaneously and which does not decay in the period of preparation. S_1–S_n absorptions of 1-methylphenanthrene in cyclohexane meet these

requirements. For these transient absorptions the matching of $R_s(\Delta t)$, by variation of σ, to $R(\Delta t)$ yields a value for 2σ of 7 ± 1 ps.

A modification in the experiments described above allows broad spectral band detection as a function of Δt. Then the continuum reference and probe beams are imaged spatially separated in the focal plane of a small flat field spectrograph and their spectral contents are recorded simultaneously with an optical multichannel analyser. The transient absorption spectrum is calculated from the spectra recorded with and without a photolysing pulse.

Figure 3 shows an outline of the spectrometer used for time-resolved absorption spectroscopy with nanosecond resolution. A pulsed Nd^{3+} glass laser system provides a primary excitation pulse with a width of 15 ns FWHM and a wavelength of either 353 or 265 nm. A beam splitter in front of the sample cell reflects about 8% of the photolysing laser pulse onto a vacuum photodiode to monitor the variation in pulse energy from shot to shot. The output of the photodiode is integrated in a gated integrator and stored digitally. The excited volume of the sample within the first 3 mm behind the entrance window for the laser pulse is traversed perpendicular to the laser beam by a relatively weak probing beam, derived from a pulsed 450 W xenon lamp burning at a low d.c. level. The lamp provides a flash with a maximum intensity which remains constant within 2% for a period of 10 μs as shown in Figs. 3(b) - 3(d) [12, 13]. The photomultiplier used to

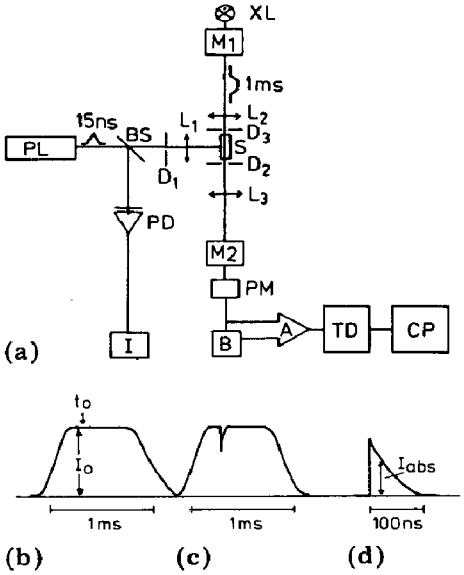

Fig. 3. (a) Spectrometer for nanosecond kinetic spectroscopy using the third or fourth optical harmonic frequency of a *Q*-switched Nd^{3+} glass laser (PL, pulsed laser; BS, beam splitter; D, diaphragm; L, lens; M, monochromator; XL, pulsed xenon lamp; S, sample cell; PM, photomultiplier; B, pulse height measurement; A, differential amplifier; TD, transient digitizer; CP, computer PDP 11/10; PD, photodiode; I, integrator); (b) pulse from the xenon lamp at time t_0 when the laser is triggered; (c) detection light pulse with induced absorption; (d) output from differential amplifier, *i.e.* the absorption signal.

detect the probing light transmitted through the sample is either an RCA type IP28 or 4840. Only the first five dynodes are used for electron multiplication and the sixth dynode is used as a quasi-anode. All other dynodes are connected directly to the anode which is maintained at +400 V relative to the sixth dynode by means of a separate power supply, thus avoiding space charge accumulation around the quasi-anode. The photocathode is kept at −1100 V relative to ground and the resistors of the dynode chain are each bypassed by sufficiently large charge storage capacitors, with $0.5\ \mu F \leqslant C \leqslant 20\ \mu F$, to ensure a linear response at output photocurrent pulses of up to 20 mA. In addition each dynode resistor is also bypassed by a small capacitor of about 3 nF to ensure a high frequency response of the photomultiplier. One of two different ways is followed in handling the output signal from the photomultiplier.

(1) The signal is passed through a high pass filter, essentially a high frequency 1:1 transformer with a 50 Ω coaxially shielded cable wound on a ferrite ring core [13], to a 500 MHz bandwidth input amplifier (Tektronix type 7A19) of a transient digitizer with a real-time bandwidth of 500 MHz (Tektronix type R7912). The transmittance of the high pass filter has a flat frequency response between 100 MHz and 50 kHz with a sag of less than 5% between these limits. The primary winding of the filter is terminated via a 1 Ω resistor to ground. A fraction of the input signal across the 1 Ω resistor is displayed on a storage oscilloscope, allowing a direct determination of I_0 as shown in Fig. 3. Only the transient modulation is then displayed undistorted up to $\Delta t = 1\ \mu s$. Beyond 1 μs the following method has to be used.

(2) The photomultiplier output is terminated into a 50 Ω resistor and the voltage across this resistor serves as one of the inputs of a differential input amplifier of the digitizer (Tektronix type 7A13) (Fig. 3, A). The input impedance of the amplifier is 1 MΩ. A 10 MΩ amplifier is also connected parallel to the 50 Ω termination of the photomultiplier and its output voltage enters a sample-and-hold circuit which measures the height of the probing pulse just before the laser excitation. The output of the sample-and-hold circuit is used as the second input to the differential amplifier and is also stored digitally as I_0 (Fig. 3, B). The difference between the two input signals, which is exactly equal to the transient modulation of the probing pulse, is then displayed on the digitizer. This is shown schematically in Fig. 3.

If I_t denotes the intensity of the probing beam emerging from the sample it follows readily that $I_t = I_0 - I_{abs}$. The transient optical density $D_u(\lambda, t)$ of the sample at the probing wavelength λ is therefore calculated according to

$$D_u(\lambda, t) = -\log_{10}\left\{\frac{I_0(\lambda) - I_{abs}(\lambda, t)}{I_0(\lambda)}\right\} \tag{10}$$

When non-linear absorptions of the excitation pulse by the sample are absent, the concentration of primary excited species depends linearly on the

excitation pulse energy E_{ex}. In all experiments the laser pulse energy has been kept sufficiently low to guarantee absence of non-linear absorptions. To be able to compare the transient optical densities at different wavelengths even when E_{ex} fluctuates from shot to shot, we have normalized $D_u(\lambda, t)$ with respect to E_{ex}:

$$D(\lambda, t) = \frac{D_u(\lambda, t)}{E_{ex}} \tag{11}$$

From the determination of $D(\lambda, t)$ at a number of discrete wavelengths, the profile of the transient absorption spectrum at time t follows. All the transient absorptions encountered in the present investigation decay single exponentially. The experimentally determined function $D(\lambda, t)$ is fitted numerically to a function of the form

$$f(t) = A \exp(-kt) + B \tag{12}$$

The numerical procedure is designed for fitting experimental curves with superimposed noise [14]. Both $D(\lambda, t)$ and $f(t)$ can simultaneously be displayed graphically on the computer terminal, allowing a visual judgment of the matching.

Sample solutions have been prepared in spectrograde organic solvents or H_2O. H_2O, containing $KMnO_4$, was refluxed and then distilled twice before use. When necessary, oxygen was removed from the solutions by flushing them with argon for about 20 min. This was found to be as effective in our work as repeated freeze–thaw cycles in vacuum.

Kinetic spectroscopic measurements as a function of temperature, in the range 300 K $\leqslant T \leqslant$ 373 K, were carried out by placing the sample cell in a specially designed thermostat with optical windows transmitting the laser and probing beams. The selected temperature was constant within a width of 0.1 K. For temperatures below 300 K a stainless steel cell situated in an optical cryostat has been used, which allows the probing and excitation beams to be perpendicular.

B-DINA has been prepared from *tert*-butylbenzene. In a first step *tert*-butylbenzene was nitrated to 1-*tert*-butyl-2,4-dinitrobenzene [15]. The compound 1-*tert*-butyl-2,4-dinitrobenzene was subsequently nitrated to 1-*tert*-butyl-2,4,6-trinitrobenzene [16]. Finally B-DINA was prepared from 1-*tert*-butyl-2,4,6-trinitrobenzene by analogy with the preparation of 3,5-DINA [17]. The product was purified chromatographically on SiO_2 (50:50 dichloromethane:pentane) and melts between 118.0 and 118.5 °C. Because of the potential danger of explosion the synthesis of the trinitro compound was carried out on a 2 g scale.

Perdeutero-3,5-DINA was obtained through reaction, in CD_3OD at 60 °C, of $NaOCD_3$ with 1,3,5-trinitro-2,4,6-trideuterobenzene [17]. The latter compound was prepared by reaction of 1,3,5-trinitrobenzene with NaOD and D_2O in dimethylformamide (DMF) at 100 °C [18]. It could be isolated in crystalline form after the reaction mixture was neutralized in a mixture of ice and sulphuric acid. This procedure was repeated twice, using

the isolated and purified deuterated trinitrobenzene from the previous step as the starting material.

The triplet quantum yields ϕ_T of 3,5-DINA and of B-DINA were determined by means of the sensitized E–Z isomerization of E-1,2-diphenylpropene (EDP) [19], after excitation with 366 nm light which is absorbed by the nitro compounds alone. The quantum yield ϕ_I for the isomerization of an EDP molecule in its state T_0 to Z-1,2-diphenylpropene (ZDP) is known to be 0.55 [19]. The overall quantum yield ϕ_Z of the sensitized isomerization is given by

$$\frac{\phi_I}{\phi_Z} = \frac{1 + k/k_T C_{EDP}}{\phi_T} \tag{13}$$

where k is the rate constant for decay of the unperturbed triplet state of the nitro compound and k_T is the rate constant for energy transfer between the nitro compound in its triplet state and EDP. The values of ϕ_T and k/k_T are obtained from a plot of ϕ_I/ϕ_Z against $1/C_{EDP}$. During the irradiation of B-DINA a photoproduct is formed which absorbs at the excitation wavelength. We have corrected for this absorption in the following way. Both the amount of ZDP and of B-DINA are determined by gas–liquid chromatography analyses as a function of irradiation time. From the amount of B-DINA that disappeared we calculated the actual amount of excitation light absorbed by B-DINA. With this procedure we obtained $\phi_T = 0.43$ and $k/k_T = 0.13$ mol l^{-1} for B-DINA. For 3,5-DINA we obtained $\phi_T = 0.45$ and $k/k_T = 0.53 \times 10^{-3}$ mol l^{-1}. It may be noted here that the rate of disappearance of B-DINA does not depend on C_{EDP}. This means that the photoproduct is formed directly from the S_1 state of B-DINA. The quantum yield ϕ_{PP} of the photoproduct is estimated to be about 0.01.

3. Results and discussion: picosecond relaxation and reaction of excited nitroanisoles

3.1. Relaxation of 3,5-dinitroanisole in non-hydrogen-bonding solvents

In a previous paper [11] a broad (4700 cm^{-1}) transient absorption band around 435 nm has been reported for 3,5-DINA and 3-NA in aqueous solutions on excitation by a 353 nm pulse. The band has been identified as an absorption from the thermally equilibrated hydrogen-bonded lowest triplet state. At that time we had no evidence that 3,5-DINA also forms a triplet state on excitation in non-hydrogen-bonding solvents. The excitation and probe technique with picosecond light pulses has enabled us to determine a transient absorption band around 450 nm in solutions of 3,5-DINA in several non-hydrogen-bonding solvents, which as we shall see has to be attributed to a $T_n \leftarrow T_0$ absorption. The weak absorption band detected in a solution of 3,5-DINA in CH_3CN after excitation at 353 nm with a pulse of 7 ps duration is presented in Fig. 4. The decay of this transient absorption was monitored at 433 nm in the time range between 0 and 1500 ps after

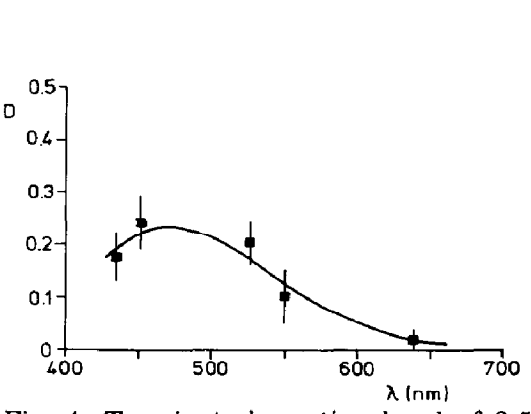

Fig. 4. Transient absorption band of 3,5-DINA in CH_3CN measured at $\Delta t \approx 20$ ps after excitation with 353 nm.

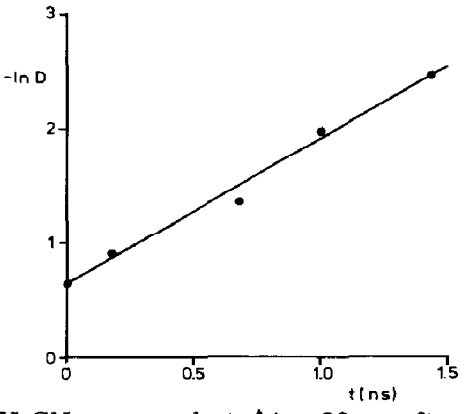

Fig. 5. Decay of the transient absorption of 3,5-DINA in CH_3CN observed at 433 nm.

initial excitation. The transient optical density $D(\Delta t) = R(\Delta t)$ decays single exponentially as a function of Δt as shown in Fig. 5. The concentration of excited species can be described by

$$C_E(t) = C_0 \exp(-k_7 t) \tag{14}$$

where $C_E(t)$ is the concentration of excited species as a function of time, C_0 the concentration of excited species directly after excitation and k_7 their decay rate constant. The single-exponential decay means that the absorption arises from a single species, *i.e.* one type of molecule in a single electronic state, at least for $\Delta t > 30$ ps. The observed lifetime $\tau = 1/k_7 = 780$ ps of the transient absorption seems incompatible with an absorption from an electronically excited singlet state, because the fluorescence quantum yield is less than 10^{-4}. From

$$\phi_F = \frac{k_r}{k_r + k_{nr}} = k_r \tau < 10^{-4} \tag{15}$$

it follows that $k_r < 10^5\ s^{-1}$ when $\tau = 780$ ps. In contrast, the radiative rate constant for the $S_0 \leftarrow S_1$ transition can be estimated from the known value of the molar extinction coefficient of the $S_1 \leftarrow S_0$ transition. With $\epsilon = 100$, k_r is found to be $10^6\ s^{-1}$. Therefore an identification of the transient absorption as an $S_n \leftarrow S_1$ absorption does not seem possible.

If the transient is identified with the triplet state of 3,5-DINA, then the triplet state lifetime k determined from the energy transfer experiment, mentioned in Section 2, should be equal to the lifetime of the transient absorption. An estimate of k can be obtained if the energy transfer between 3,5-DINA and EDP is assumed to be diffusion controlled; k_T can then be taken to be equal to $k_{diff} \approx 1.9 \times 10^{10}\ l\ mol^{-1}\ s^{-1}$, from which a value k of about $2 \times 10^9\ s^{-1}$ results [20]. This is close to the decay rate constant k_7 of the transient absorption of $1.28 \times 10^9\ s^{-1}$. Hence the absorption may be identified as a $T_n \leftarrow T_0$ absorption of 3,5-DINA.

The triplet lifetime of 780 ± 100 ps is extremely short. Only for nitrobenzene in isopropanol has a triplet lifetime of the order of magnitude of 1 ns been estimated from quenching experiments [21].

Nitrobenzene is thought to have an $n\pi^*$ electron configuration in the lowest triplet state, which would be expected to lead to photoreduction of the NO_2 group [21, 22]. However, the quantum yield ϕ_{red} of photoreduction of nitrobenzene in isopropanol is quite low, about 10^{-2}, and this has been explained by very efficient $T_0 \rightarrow S_0$ intersystem crossing, and not by a low reactivity [21]. We may conclude that nitrobenzene and 3,5-DINA are very similar in this respect.

Weak transient absorptions of 3,5-DINA around 450 nm were not only observed in CH_3CN but also in the less polar solvents CH_2Cl_2, 2-methyltetrahydrofuran (2-MTHF) and benzene. The lifetimes of these transient absorptions have not been determined in a picosecond experiment. However, after excitation with a pulse of 15 ns duration, they are not observed using a detection system with a time resolution of 5 ns. Therefore the lifetimes must be shorter than 5 ns. If the solutions are excited with a 7 ps pulse the transient absorption rises to a maximum value within about 25 ps. No significant decay is observed during the next 100 ps. This means that the lifetime is at least 1 ns. Applying the same arguments as used for the solution in CH_3CN, we conclude that the transient absorption arises from $T_n \leftarrow T_0$ transitions, with a lifetime τ of T_0 between 1 and 5 ns. The results are summarized in Table 1.

To obtain more insight into the mechanism of the fast relaxation of 3,5-DINA, similar experiments were carried out with perdeutero-3,5-DINA. The decay of the $T_n \leftarrow T_0$ absorption at 433 nm of electronically excited d_6-3,5-DINA in CH_3CN is shown in Fig. 6, where $\ln\{D(\Delta t)\}$ is plotted *versus* the delay time Δt. From this plot the lifetime of T_0 of d_6-3,5-DINA is found to be 880 ± 120 ps. Therefore, we may conclude that deuteration does not change the lifetime of T_0 of 3,5-DINA in CH_3CN significantly. Apparently the C—H vibrations are not important as accepting and/or promoting modes in the radiationless decay of the triplet state of 3,5-DINA. Since the height of the plateau in $D(t)$ reached at time t_m (Fig. 7) also does not change with isotope substitution, it must be concluded that the quantum yield of triplet formation is not affected. This means that the rate of intersystem crossing $S_1 \rightarrow T_0$ and the rate of internal conversion $S_1 \rightarrow S_0$ either both change with the same factor or do not change at all. The latter possibility is the more acceptable since the decay of T_0 is also independent of isotope substitution.

We have measured the growth of the transient absorption of 3,5-DINA and the other nitroanisoles in a number of solutions. We shall first examine how the rate constants of the different relaxation processes can be determined from these growth curves. The populating kinetics of the triplet state can be derived from $R(\Delta t)$ in the interval -10 ps $< \Delta t < 100$ ps. Simulation of $R(\Delta t)$ requires the specification of a kinetic scheme describing the relaxation processes of the primary excited singlet state and the triplet state. The scheme which we use here is depicted in Fig. 8. A single rate constant k_2 is

TABLE 1

Rate constants for 3,5-dinitroanisole in non-hydrogen-bonding solvents

Solvent	ϵ_S/ϵ_T	k_1 ($\times 10^{11}$ s^{-1})	k_2 ($\times 10^{11}$ s^{-1})	k_7 ($\times 10^9$ s^{-1})	ϕ_T
CH_3CN	0.0	1.0	0.80	1.28	0.45
	0.2	0.80	0.64	1.28	0.45
	0.3	0.60	0.50	1.28	0.45
	0.4	n	n	1.28	0.45
CH_2Cl_2	0.0	3.2	0.8	0.2 - 1	0.22 [a]
	0.1	1.6	0.4	0.2 - 1	0.22
	0.2	n	n	0.2 - 1	0.22
2-MTHF [b]	0.0	0.5	0.4	0.2 - 1	0.4 [a]
	0.2	0.4	0.33	0.2 - 1	0.4
	0.3	n	n	0.2 - 1	0.4
Benzene	—	—	—	0.2 - 1	$\approx$ 0.2 [a]

n, no good fit can be obtained.
[a] Estimated from $D(t_m)$ relative to CH_3CN.
[b] Measured at 26 and 70 K (all other experiments were performed at room temperature).

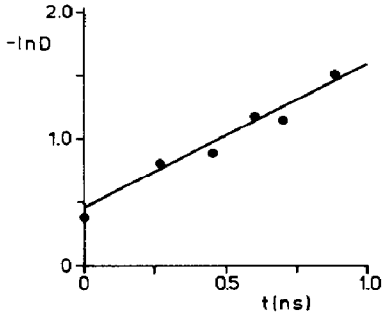

Fig. 6. Decay of the $T_n \leftarrow T_0$ absorption of d_6-3,5-DINA in CH_3CN at 433 nm.

introduced to describe the intersystem crossing process $S_1 \rightarrow T_0$. Similarly the internal conversion process $S_1 \rightarrow S_0$ is described by k_1. The time dependence of the concentrations $C_S(t)$ and $C_T(t)$ of singlet and triplet excited states are given by the following differential equations:

$$\frac{dC_S(t)}{dt} = \alpha I_{ex}(t) - (k_1 + k_2)C_S(t) \tag{16}$$

$$\frac{dC_T(t)}{dt} = k_2 C_S(t) - k_7 C_T(t) \tag{17}$$

in which α is a proportionality constant depending on the optical density at the excitation wavelength of the ground state molecules. The rate constant k_7 describes the decay of T_0. In almost all cases this decay can be neglected because it is much slower than the rate of formation of T_0. With $C_S(-\infty) = C_T(-\infty) = 0$ as boundary conditions, the following solutions of eqns. (16) and (17) are obtained:

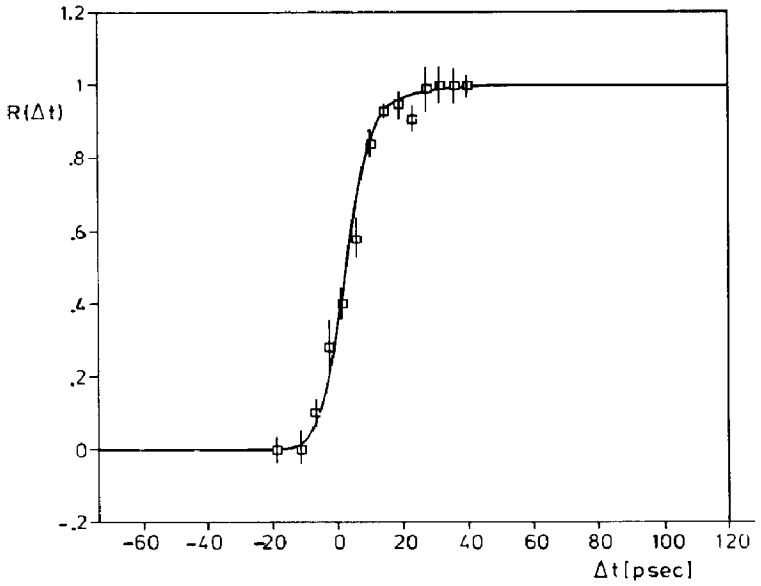

Fig. 7. Transient absorption of 3,5-DINA in CH_3CN at 435 nm after excitation at 353 nm. The curve was calculated with $\epsilon_S/\epsilon_T = 0$, $k_1 = 1.0 \times 10^{11}\ s^{-1}$ and $k_2 = 8.0 \times 10^{10}\ s^{-1}$.

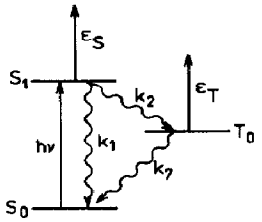

Fig. 8. Kinetic scheme used to simulate growth and decay of transient absorptions in non-hydrogen-bonding solvents: ⟶, optical transitions; ⇝, non-radiative transitions.

$$C_S(t) = \alpha \int_{-\infty}^{t} I_{ex}(t') \exp\{-(k_1 + k_2)(t - t')\}\, dt' \tag{18}$$

$$C_T(t) = k_2 \int_{-\infty}^{t} C_S(t') \exp\{-k_7(t - t')\}\, dt' \tag{19}$$

When we assume that the measuring light is only absorbed by S_1 and T_0, the optical density can be calculated from

$$D(t) = \epsilon_S C_S(t) + \epsilon_T C_T(t) \tag{20}$$

In eqn. (20) ϵ_S and ϵ_T are considered to be independent of time. A time dependence due to vibrational relaxation in the excited states can be envisaged [23, 24]. This effect will be neglected because usually the vibrational relaxation is already completed on the time scale considered here [25].

A numerical simulation of $R(\Delta t)$ is performed by using eqns. (18) - (20) and eqns. (1) - (9). The variables in the simulation are k_1, k_2 and ϵ_S/ϵ_T. The pulse width of 7 ± 1 ps and k_7 have already been determined. A close match of the calculated curve to the experimental values of $R(\Delta t)$ is obtained after

a stepwise variation in k_1, k_2 and ϵ_S/ϵ_T. In some instances there is no unique solution for the set of variables and then the choice of the most acceptable solution has to rely on consistency with other facts. Such an additional constraint is the triplet quantum yield, which fixes the ratio k_1/k_2. In Fig. 7 we show the experimental points $R(\Delta t)$ and a simulated curve for 3,5-DINA in CH_3CN. The values of $R(\Delta t)$ have been determined at 435 nm and 300 K. The quantum yield for triplet formation of 3,5-DINA in CH_3CN, *i.e.* ϕ_T = 0.45, is used as a constraint. The simulations show that the contributions of $S_n \leftarrow S_1$ absorption is small compared with the contribution of the $T_n \leftarrow T_0$ absorption. Table 1 gives the values of the parameters k_i and ϵ_S/ϵ_T, which give a good fit between the calculated curve and the experimental points. For each value of ϵ_S/ϵ_T between 0 and 0.3 we find values for k_1 and k_2 which give a good fit to the experimental points. The curve shown in Fig. 7 is obtained with $\epsilon_S/\epsilon_T = 0$. It can be seen in Table 1 that via the simulation limits are obtained between which k_1, k_2 and ϵ_S/ϵ_T may vary. The following ranges are observed: $0 < \epsilon_S/\epsilon_T < 0.3$; $6 \times 10^{10}\ s^{-1} \leqslant k_1 \leqslant 10 \times 10^{10} s^{-1}$; $5 \times 10^{10}\ s^{-1} \leqslant k_2 \leqslant 8 \times 10^{10}\ s^{-1}$.

Figure 9 refers to experimental points $R(\Delta t)$ and a calculated curve for a solution of 3,5-DINA in CH_2Cl_2. Again $R(\Delta t)$ has been measured at 435 nm. The stationary value of $R(\Delta t)$, *i.e.* $D(t_m)$ ($\Delta t > 100$ ps), is a measure of the quantum yield of triplet formation

$$D(t_m) \propto \epsilon_T \phi_T \tag{21}$$

If ϵ_T is independent of the solvent we may use $D(t_m)$ as a measure for ϕ_T. It is to be expected that the value of ϵ_T will change little due to a solvent-induced bandshift in going from CH_3CN to CH_2Cl_2 as a solvent because the

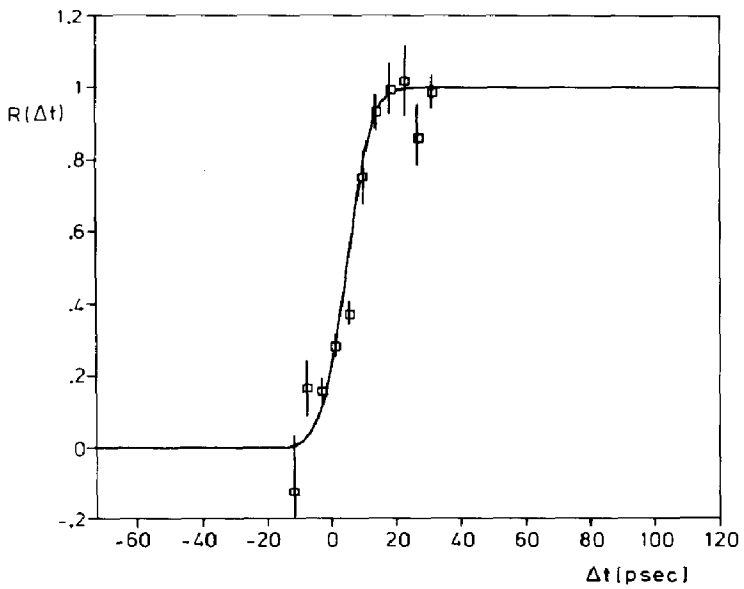

Fig. 9. Transient absorption of 3,5-DINA in CH_2Cl_2 at 435 nm and curve calculated with $\epsilon_S/\epsilon_T = 0$, $k_1 = 3.2 \times 10^{11}\ s^{-1}$ and $k_2 = 8.0 \times 10^{10}\ s^{-1}$.

observed $T_n \leftarrow T_0$ absorption band of 3,5-DINA in CH_3CN is rather flat and broad around 435 nm. The value of $D(t_m)$ in CH_2Cl_2 amounts to 50% of that observed in CH_3CN. Therefore the triplet quantum yield in CH_2Cl_2 is estimated to be

$$\phi_{T,\,CH_2Cl_2} = 0.5 \times \phi_{T,\,CH_3CN} \approx 0.22$$

The rate constants obtained with this value of ϕ_T are also given in Table 1.

When we compare the rate constants obtained in solutions of 3,5-DINA on going from CH_3CN to CH_2Cl_2 at a fixed ratio of ϵ_S/ϵ_T it is observed that k_1 increases. In fact, for $\epsilon_S/\epsilon_T = 0$, k_1 increases by a factor of 3.2 whereas k_2 remains constant. The higher rate of internal conversion $S_1 \rightarrow S_0$ leads to a lower triplet quantum yield. This seems to apply to 3,5-DINA in benzene for which we again observe a transient absorption with an estimated quantum yield lower than in CH_3CN. Therefore it might be thought that the increase in the internal conversion rate is related to the decrease in polarity of the solvent in going from CH_3CN to CH_2Cl_2 and benzene.

The influence of temperature on the kinetics of triplet state population has been studied in a glassy solution of 3,5-DINA in 2-MTHF at 70 and 26 K. The growth curves of the transient absorption are shown in Fig. 10.

The curve through the points is obtained with $\epsilon_S/\epsilon_T = 0$, $k_1 = 5.0 \times 10^{10}\ s^{-1}$ and $k_2 = 4.0 \times 10^{10}\ s^{-1}$. The triplet quantum yield is estimated from $D(t_m)$ to be 0.4, which is used as a constraint in the fitting. Rate constants determined for different values of ϵ_S/ϵ_T are included in Table 1. From the measurements it follows that the rate constants k_1 and k_2 do not change on increasing the temperature from 26 to 70 K. Since ϕ_T, estimated from $D(t_m)$, also does not change with increase in temperature from 70 K to room temperature, it might be concluded that k_1 and k_2 are temperature indepen-

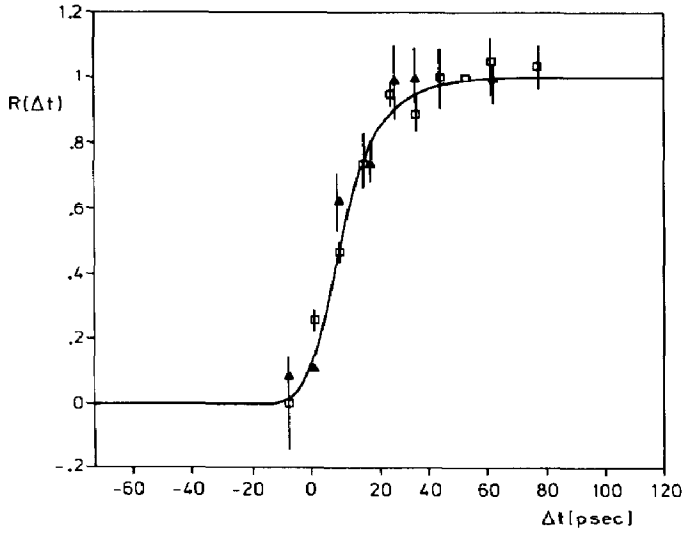

Fig. 10. Transient absorption of 3,5-DINA in 2-MTHF at 435 nm measured at 26 K (▲) and 70 K (□). The curves giving the best fit for each temperature coincide.

dent within the range from 26 to 300 K. This behaviour may be expected if the exchange of vibrational energy between the solvent and the excited solute is slower than the electronic relaxation, but it could also be due to strong phonon coupling in the electronic relaxation as explained in Section 3.7.

3.2. Relaxation of 3,5-dinitroanisole in hydrogen bonding solvents

The observation of a long-lived hydrogen-bonded triplet state of 3,5-DINA in aqueous solvent systems raises several questions [11]. For instance, in which of its excited states does 3,5-DINA react with a solvent molecule to form a hydrogen bond and how does the hydrogen bond affect the radiationless decay? To find an answer to such questions we have measured transient absorption spectra on a picosecond time scale of 3,5-DINA in aqueous solvent mixtures and in alcohols. Also the growth and decay of the transients have been monitored. As solvents we chose mixtures of CH_3CN and H_2O because of the influence of the composition of this solvent system on the triplet lifetime, which suggests that also the rates of triplet formation may be influenced.

In Fig. 11 the long wavelength part of the transient absorption is shown as it is observed with the optical multichannel analyser at Δt = 20 ps. This part of the spectrum is identical with that observed in the same wavelength region at Δt = 5 ns. Obviously it does not contain an $S_n \leftarrow S_1$ absorption band. Because ϕ_T of 3,5-DINA varies from 0.45 in pure CH_3CN to 0.9 in pure H_2O [6] it is expected that the maximum optical density $D(t_m)$ after excitation likewise depends on the solvent composition. The maximum optical density $D(t_m)$ at 430 nm for various mixtures of CH_3CN and H_2O is shown in Fig. 12. An increase in $D(t_m)$ by a factor of 3 is observed in going from CH_3CN to H_2O, while at the same time ϕ_T changes by a factor of 2. If all triplet states are hydrogen bonded in aqueous solutions then this means that the molar extinction coefficient at 430 nm of the hydrogen-bonded triplet species must be 1.5 times larger than that of the non-hydrogen-bonded species. We think that this change is too large to be caused by a solvent-induced band shift, since the absorption band is rather flat around 430 nm. However, the interchange of $^3\pi\pi_1^*$ and $^3n\pi_1^*$ states, which we think occurs in

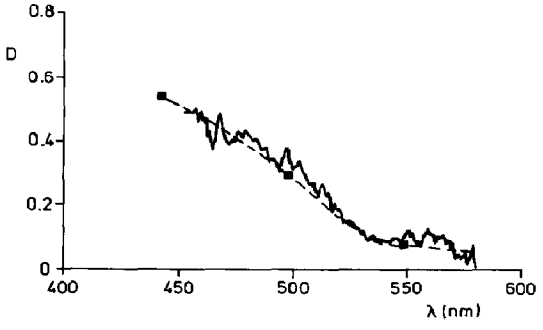

Fig. 11. Transient absorption band of 3,5-DINA in CH_3CN–H_2O directly after excitation and the $T_n \leftarrow T_0$ absorption band (— — —) measured after 10 ns.

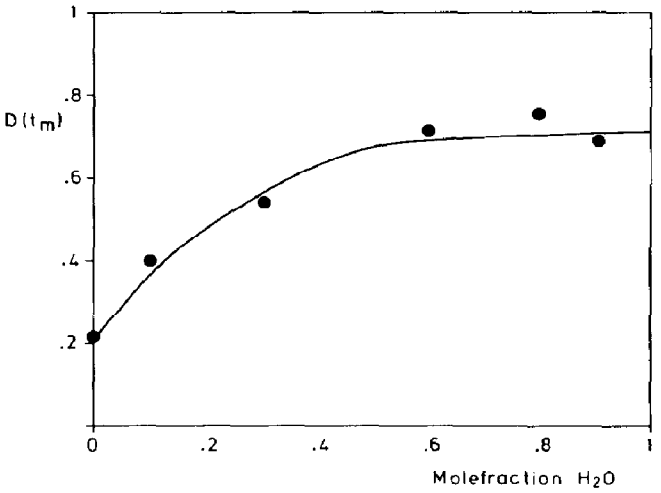

Fig. 12. Maximum optical density of 3,5-DINA at 430 nm directly after excitation ($\Delta t \approx$ 30 ps) as a function of H_2O concentration in a solution of 3,5-DINA in H_2O–CH_3CN mixtures.

hydrogen bonding solvents, could explain this increase in ϵ_{T_0}. The growth curves $R(\Delta t)$ at 433 nm for solutions of 3,5-DINA in three different CH_3CN–H_2O mixtures are given in Fig. 13. In addition to the changes in $D(t_m)$ mentioned above, we observe a remarkable change in the rise time τ_r. The rise time increases with the water content of the mixtures. The greatest increase occurs in the region $0 \leqslant \chi_{H_2O} \leqslant 0.4$, which is also the interval where the greatest change in $D(t_m)$ is observed.

There are a number of reasons why the simple kinetic scheme for triplet formation introduced before cannot be used to simulate the observed kinetics. We have evidence from IR studies that 3,5-DINA in its electronic ground state does not even form hydrogen bonds with 2,2,2-trifluoroethanol (TFE); this and other results have led to the conclusion that 3,5-DINA is *non*-hydrogen-bonded in its ground state in aqueous solutions. The triplet state of 3,5-DINA, however, is thought to be hydrogen bonded in aqueous solutions. Therefore a hydrogen bonding reaction between the excited 3,5-DINA and a solvent molecule should be incorporated in the relaxation scheme. We shall now discuss the kinetic scheme we have used to interpret the $R(\Delta t)$ curves and the behaviour of $D(t_m)$ observed in aqueous solutions of various compositions. The most general scheme takes into account the initially excited singlet state S_i and triplet state T_0 of the non-hydrogen-bonded molecules, as well as the excited singlet $S_{i,HB}$ and triplet $T_{0,HB}$ states of the hydrogen-bonded molecules. Species are considered to have distinct extinction coefficients.

The relaxation processes that may be operative are labelled as follows: k_1 for internal conversion, $S_i \rightarrow S_0$; k_2 for intersystem crossing, $S_i \rightarrow T_0$; k_3 for reaction with H_2O, $S_i \rightarrow S_{i,HB}$; k_4 for intersystem crossing, $S_{i,HB} \rightarrow T_{0,HB}$; k_5 for internal conversion, $S_{i,HB} \rightarrow S_0$; k_6 for reaction with H_2O, $T_0 \rightarrow T_{0,HB}$; k_7 for intersystem crossing, $T_0 \rightarrow S_0$; k_8 for intersystem crossing,

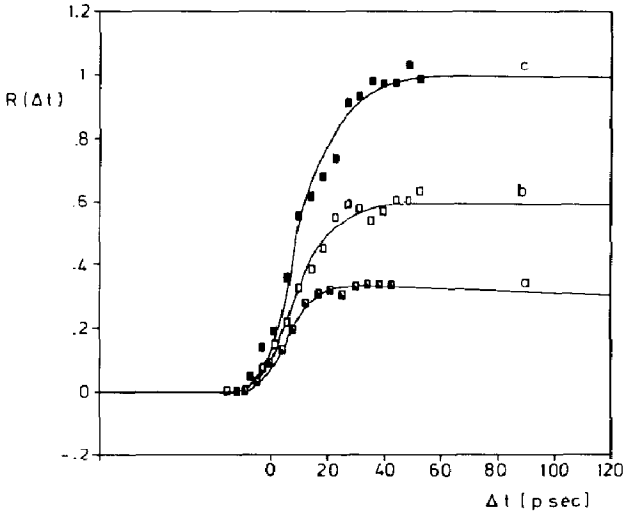

Fig. 13. Growth curves of the transient absorption of 3,5-DINA at 430 nm in CH_3CN–H_2O mixtures with various mole fractions of H_2O: curve a, $\chi_{H_2O} = 0$; curve b, $\chi_{H_2O} = 0.13$; curve c, $\chi_{H_2O} = 0.80$.

$T_{0,HB} \rightarrow S_{0,HB}$. The constants k_5 and k_8 refer to overall rates; it is not important whether the relaxation processes lead directly to a dissociated complex or not. The model takes into account that thermally activated dissociation of the hydrogen bond(s) in $S_{i,HB}$ and $T_{0,HB}$ does not occur in the time interval $0 \text{ ps} \leqslant \Delta t \leqslant 80$ ps. This is in accordance with the results presented in Section 4.3.

The model implies the following differential equations:

$$\frac{dC_{S_i}(t)}{dt} = \alpha I_{ex}(t) - (k_1 + k_2 + k_3)C_{S_i}(t)$$

$$\frac{dC_{S_{i,HB}}(t)}{dt} = k_3 C_{S_i}(t) - (k_4 + k_5)C_{S_{i,HB}}(t)$$

$$\frac{dC_{T_0}(t)}{dt} = k_2 C_{S_i}(t) - (k_6 + k_7)C_{T_0}(t) \qquad (22)$$

$$\frac{dC_{T_{0,HB}}(t)}{dt} = k_4 C_{S_{i,HB}}(t) + k_6 C_{T_0}(t) - k_8 C_{T_{0,HB}}(t)$$

With the initial conditions $C_i(-\infty) = 0$, the solutions are

$$C_{S_i}(t) = \alpha \int_{-\infty}^{t} I_{ex}(t') \exp\{-(k_1 + k_2 + k_3)(t - t')\}\, dt'$$

$$C_{S_{i,HB}}(t) = k_3 \int_{-\infty}^{t} C_{S_i}(t') \exp\{-(k_4 + k_5)(t - t')\}\, dt' \qquad (23)$$

$$C_{T_0}(t) = k_2 \int_{-\infty}^{t} C_{S_i}(t') \exp\{-(k_6 + k_7)(t - t')\}\, dt'$$

$$C_{T_0,HB}(t) = \int_{-\infty}^{t} \{k_4 C_{S_i,HB}(t') + k_6 C_{T_0}(t')\} \exp\{-k_8(t - t')\}\, dt' \qquad (23)$$

$$D(t) = \epsilon_{S_i} C_{S_i}(t) + \epsilon_{T_0} C_{T_0}(t) + \epsilon_{S_i,HB} C_{S_i,HB}(t) + \epsilon_{T_0} C_{T_0}(t) \qquad (24)$$

To be tractable the above general model needs simplification, despite the fact that some of the rate constants are already known. We shall now show how this has been done, and how it results in the kinetic scheme shown in Fig. 14.

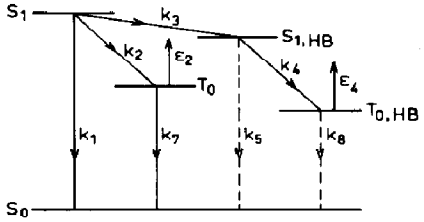

Fig. 14. Kinetic scheme for relaxation of electronically excited 3,5-DINA in hydrogen bonding solvents: — — —, processes too slow to interfere with kinetic behaviour on a picosecond time scale.

The intramolecular relaxation rate constants k_1, k_2 and k_7 of the *non*-hydrogen-bonded molecules have already been determined for solutions of 3,5-DINA in CH_3CN. They are not expected to depend significantly on the composition of the CH_3CN–H_2O mixtures, since the major influence would arise from the change in the dielectric constant of the solvent, and the reaction field due to solvent polarization by the excited state changes very little in going from CH_3CN to H_2O. Figure 12 shows that the greatest changes in $D(t_m)$ relative to CH_3CN occur at $\chi_{H_2O} = 0.4$ where the dielectric constant does not vary much. Therefore we assign to k_1, k_2 and k_7, of the *non*-hydrogen-bonded 3,5-DINA molecules in the CH_3CN–H_2O mixtures, the same values as those obtained in CH_3CN.

The non-hydrogen-bonded triplet state T_0 of 3,5-DINA probably is an $n\pi^*$ state. In this state the molecule will have even less tendency to form hydrogen bonds than in the ground state. Consequently the rate constant k_6, representing the reaction of T_0 with the solvent molecules, will be taken as equal to zero.

Since the rise time of $R(\Delta t)$ is more than twice as long in CH_3CN–H_2O mixtures than in CH_3CN, the contribution of an $S_n \leftarrow S_1$ absorption to the total absorption must be even smaller than in CH_3CN. In CH_3CN the best fit was obtained with $\epsilon_S = 0$; therefore we take $\epsilon_{S_i} = \epsilon_{S_i,HB} = 0$ in the simulation of $R(\Delta t)$ in CH_3CN–H_2O mixtures.

Consequently also the values of the rate constants k_1 and k_2 obtained with $\epsilon_{S_i} = 0$ for the solution in CH_3CN must be used.

An estimate of k_5 follows from the quantum yield for triplet formation. In CH_3CN–H_2O mixtures with $\chi_{H_2O} = 0.6$, the triplet quantum yield ϕ_T of 3,5-DINA reaches a value of 0.9 [6].

The scheme in Fig. 14 implies

$$\phi_{T,HB} = \phi_1 \times \phi_2 \tag{25}$$

with

$$\phi_1 = \frac{k_3}{k_1 + k_2 + k_3}$$

$$\phi_2 = \frac{k_4}{k_4 + k_5} \tag{26}$$

With $\phi_{T,HB} = 0.9$, from eqn. (25) $\phi_1 \geqslant 0.9$ and $\phi_2 \geqslant 0.9$ and therefore $k_5/k_4 \leqslant 1/9$ for $0.6 \leqslant \chi_{H_2O} \leqslant 1.0$. Therefore $k_5 = 0$ can be used in the calculation of $R(\Delta t)$. It will be assumed that $k_5 = 0$ also applies for the hydrogen-bonded molecule in solvent mixtures with $\chi_{H_2O} < 0.6$. The ratio $\epsilon_{T_0}/\epsilon_{T_0,HB}$ follows from $D(t_m)$ determined for solutions of 3,5-DINA in CH_3CN and in CH_3CN–H_2O mixtures with $\chi_{H_2O} > 0.6$ and the known triplet quantum yields in these solutions. Using eqn. (21), we find

$$\epsilon_{T_0}/\epsilon_{T_0,HB} = 2.3$$

The rate constants k_7 and k_8 for intersystem crossing from the triplet states to the ground state are known experimentally: $k_7 = 1.28 \times 10^9\ s^{-1}$ and $k_8 < 10^6\ s^{-1}$, and they may therefore be neglected.

We can now summarize the assigned values of the rate constants and extinction coefficients: (1) $k_1 = 1.0 \times 10^{11}\ s^{-1}$, $k_2 = 0.8 \times 10^{11}\ s^{-1}$ (these values are the same as in neat CH_3CN); (2) $\epsilon_{S_i} = \epsilon_{S_i,HB} = 0$; (3) $k_5 = 0$ (this follows from $\phi_T = 0.9$ for solutions with $\chi_{H_2O} > 0.6$); (4) $k_6 = 0$ ($^3n\pi_1^*$ does not form hydrogen bonds).

The simplified kinetic scheme retains only three decay channels: two already existing in non-hydrogen-bonding solvents and a third one via the hydrogen-bonded excited singlet state. The rate constants that still have to be determined are the rate constant k_3 for hydrogen bonding with S_i and k_4 the rate constant for intersystem crossing in the hydrogen-bonded molecule.

The simulations show that the formation of the hydrogen-bonded excited singlet state is no longer the rate-determining step in solvent mixtures with $\chi_{H_2O} > 0.6$. Qualitatively this is explained in the following way. The triplet quantum yield is 0.9 when $\chi_{H_2O} > 0.6$. Therefore k_3 must be much larger than k_2. If then k_3 would be the rate-limiting step, then the rise time of $R(\Delta t)$ would be shorter than that observed in CH_3CN. However, the actual rise time in the mixed aqueous solvents is slower than in CH_3CN. Therefore the intersystem crossing process $S_{i,HB} \rightarrow T_{0,HB}$ is the rate-limiting step in mixed aqueous solvents with $\chi_{H_2O} > 0.6$. With the parameters given in

TABLE 2

Rate constants for 3,5-dinitroanisole in hydrogen bonding solvents

Solvent	k_1 ($\times 10^{11}$ s^{-1})	k_2 ($\times 10^{11}$ s^{-1})	k_3 ($\times 10^{11}$ s^{-1})	k_4 ($\times 10^{11}$ s^{-1})	k_7 ($\times 10^{11}$ s^{-1})	k_8 ($\times 10^{11}$ s^{-1})	$\epsilon_{T_0}/\epsilon_{T_0,HB}$
CH_3CN-H_2O							
$\chi_{H_2O} = 0$	1.0	0.8	0	—	0.012	—	—
$\chi_{H_2O} = 0.13$	1.0	0.8	1.4	0.8	0.012	0.005	0.66
$\chi_{H_2O} = 0.44$	1.0	0.8	5	0.8	0.012	$\ll 0.005$	0.66
$\chi_{H_2O} = 0.60$	1.0	0.8	≥ 5	0.8	0.012	$\ll 0.005$	0.66
$\chi_{H_2O} = 0.80$	1.0	0.8	≥ 5	0.8	0.012	$\ll 0.005$	0.66
TFE	1.0	0.8	≥ 5	0.8	0	0	0.66
HFP-2	—	—		≥ 0.8 [a]	—	—	—

$k_5 = k_6 = 0$ in all simulations.

[a] Estimate based on equality of $R(\Delta t)$ curves of 3,5-DINA in H_2O and in 1,1,1,3,3,3-hexafluoropropanol-2 (HFP-2), measured with a lower time resolution of 25 ps.

Table 2, $k_4 = 8 \times 10^{10}$ s^{-1} is obtained. This is close to the value of k_2 for a solution in CH_3CN. If $\chi_{H_2O} < 0.6$ then T_0 and $T_{0,HB}$ will both contribute to the transient absorption. With $k_4 = 8 \times 10^{10}$ s^{-1}, k_3 is calculated from the $R(\Delta t)$ curves obtained in CH_3CN-H_2O mixtures with $\chi_{H_2O} < 0.6$. The values obtained in this way are given in Table 2.

The reaction rate constant k_3 is found to depend on the concentration of H_2O in the solvent mixture. This dependence shows that the reaction of S_i with H_2O is approximately first order. For a first-order reaction, $k_3 = \beta[H_2O]$ s^{-1}. We find that $\beta = 3 \times 10^{10}$ l mol^{-1} s^{-1} which is close to what is expected for a diffusion-limited reaction in CH_3CN. The description of k_3 as limited by diffusion is of course much more satisfactory in solvent mixtures that contain a relative low amount of H_2O than for H_2O-rich solutions.

The value of $D(t_m)$ can be calculated as a function of k_3 according to

$$D(t_m) = \frac{(k_2 + 1.5k_3)\epsilon_{T_0}}{k_1 + k_2 + k_3} \tag{27}$$

The calculated curve matches the experimental $D(t_m)$ values, as is shown in Fig. 12. A conclusion to be drawn from the shape of the $D(t_m)$ curve is that k_6, the rate constant for the reaction of H_2O with T_0, must be zero. When $k_6 \neq 0$ a different functional relationship between $D(t_m)$ and k_3 applies:

$$D(t_m) = \frac{1.5(k_2 + k_3)}{k_1 + k_2 + k_3}\epsilon_{T_0} \tag{28}$$

In this case a sharp increase in $D(t_m)$ with increasing H_2O content results for low concentrations of H_2O in CH_3CN-H_2O mixtures.

The close agreement between the experiment and eqn. (27) serves as an additional argument to identify T_0 with an $n\pi^*$ triplet state, incapable of forming hydrogen bonds.

Summarizing we come to the following conclusions on the relaxation of 3,5-DINA in aqueous solutions.

(a) Hydrogen bond formation with 3,5-DINA in its S_i state competes with radiationless relaxation from S_i via k_1 and k_2. The hydrogen bonding reaction can be described as a first-order reaction in the concentration of H_2O, at least for solutions with $\chi_{H_2O} < 0.6$.

(b) Hydrogen bonding results in a large reduction in the rates of internal conversion $S_i \rightarrow S_0$ and of intersystem crossing $T_0 \rightarrow S_0$ to the ground state. However, it hardly affects the rate of intersystem crossing $S_i \rightarrow T_0$.

(c) The rate of growth of the transient absorption in pure CH_3CN is determined by $k_1 + k_2$. In H_2O-rich solutions it is determined mainly by k_4, because nearly all molecules in S_i become hydrogen bonded. As $k_4 = (k_1 + k_2)/2$, we observe a much slower growth of the transient absorption in H_2O-rich solutions.

We shall now investigate whether we can apply the same model to the results obtained with solutions in TFE. After excitation of a solution of 3,5-DINA in TFE a $T_n \leftarrow T_0$ absorption band similar to that in aqueous solutions is observed. The lifetime of the triplet state at 300 K here is as high as 3.5 μs and we are definitely dealing with a hydrogen-bonded triplet state. The value of $D(t_m)$ at 435 nm equals that observed in aqueous solutions; therefore we assume that the triplet quantum yield is approximately equal to that observed in H_2O, *i.e.* $\phi_T = 0.9$, for 3,5-DINA in TFE. The measurements of $R(\Delta t)$ at 433 nm give a curve similar to that observed in CH_3CN–H_2O mixtures with $\chi_{H_2O} < 0.6$. The curve has a rise time of approximately 30 ps. Application of the model from Fig. 14 with the same assumptions as in the calculation of $R(\Delta t)$ for the CH_3CN–H_2O solvents leads to the rate constants given in Table 2.

In single-component hydrogen bonding solvents the reaction of S_i with a solvent molecule can no longer be described as a diffusion-controlled reaction. Probably the time required to form the solute–solvent hydrogen bond is limited by the orientation relaxation time of the solvent molecules and/or the average lifetime of the solvent–solvent hydrogen bonds. Our experiments show that $k_3 = 5 \times 10^{10}\ s^{-1}$, which corresponds to a reaction time τ of 2.0 ps. The orientational relaxation time τ_{or} in pure H_2O amounts to 2.5 ps and in solvent mixtures of CH_3CN and H_2O it varies between 3.0 and 1.0 ps, depending on the amount of H_2O [26]. Therefore the rate constants obtained for hydrogen bond formation appear to have realistic values.

We have investigated the effect of polarization on the transient absorption kinetics for 3,5-DINA in TFE. The largest difference, if any, will be observed directly after the excitation has taken place, *i.e.* around $\Delta t = 10$ ps [27, 28]. $R(\Delta t)$ values were measured directly after excitation at 435 nm for $0\ \text{ps} < \Delta t < 10\ \text{ps}$. No difference has been observed between $R(\Delta t)_\parallel$ and $R(\Delta t)_\perp$. Therefore we conclude that no induced polarization effects occur for 3,5-DINA and that the measured kinetics of $R(\Delta t)$ are the real kinetics, which are not obscured by polarization effects.

3.3. Exciplex emission from 3,5-dinitroanisole

In solutions of 3,5-DINA in mixtures of H_2O and CH_3CN with a mole fraction of H_2O greater than 0.5 a very weak emission after excitation with a 15 ns pulse at 353 nm is observed. The uncorrected spectrum is shown in Fig. 15. Because of the very low quantum yield of this emission it is difficult to exclude impurity luminescence. Nevertheless there are several reasons to assume that this emission arises from the excited singlet state of 3,5-DINA. The solvent itself did not show any emission in the wavelength region of interest. Repeated purification of 3,5-DINA did not influence the intensity of the luminescence. When the mole fraction of H_2O in the solvent mixture decreases from about 0.6 to 0.5 the intensity of the emission decreases. Below a mole fraction of H_2O of 0.5 it can no longer be observed. In exactly the same region of solvent composition, the triplet lifetime of 3,5-DINA changes from several tens of nanoseconds to the subnanosecond range. Because the strong variation in the lifetime of the triplet state in this mole fraction region is characteristic for 3,5-DINA it seems reasonable to associate the observed luminescence with 3,5-DINA.

The intensity of the emission is linearly dependent on the excitation intensity; from this we may conclude that the emission does not originate from photoproducts that are excited by the 353 nm pulse. For such secondary processes a quadratic dependence on the excitation intensity would be observed. A possible photofragment would be the NO_2 radical, which is known to yield luminescence after excitation [29]. The lifetime of the emission is shorter than 5 ns, which is the time resolution of the detection system. In all instances the lifetime of the emission is much shorter than the lifetime of the triplet state of 3,5-DINA. Therefore we conclude that the emission arises from the excited singlet state of 3,5-DINA and not from the triplet state.

On the basis of the absorption spectrum a fluorescence band is expected to occur around 400 nm; however, the maximum of the emission is around 570 nm. Both the large red shift and the broad structureless shape point to exciplex emission [30]. Here the exciplex could be the complex between 3,5-DINA in its $\pi\pi^*$ charge transfer state and an H_2O molecule. The

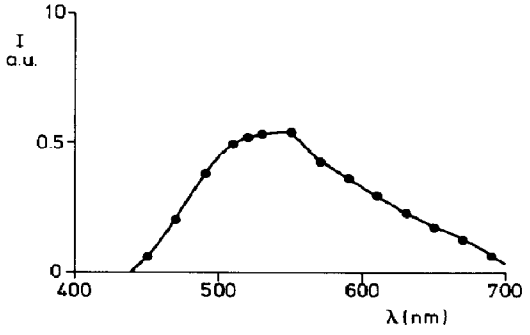

Fig. 15. Emission spectrum of 3,5-DINA observed after excitation with a 353 nm high intensity laser pulse in CH_3CN–H_2O mixtures with $\chi_{H_2O} > 0.5$.

emission originates then from the complex and terminates in a dissociative ground state, as shown in Fig. 16. From the intensity we estimate an upper limit of the quantum yield ϕ_F of fluorescence of 10^{-4} or less. With $k_{nr} = 10^{11}\ s^{-1}$ and $\phi_F = k_F/k_F + k_{nr}$ we obtain $k_F = 10^7\ s^{-1}$. This is not unreasonable for a $\pi\pi^*$ transition which has a molar extinction coefficient ϵ_{max} of 3000 l $mol^{-1}\ cm^{-1}$.

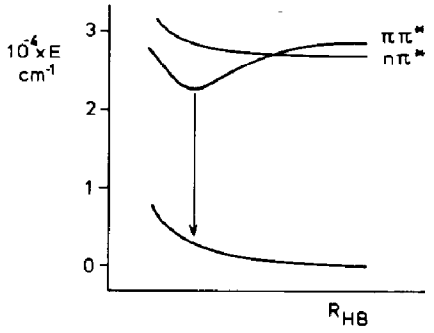

Fig. 16. Conceivable shape of potential energy surfaces of the singlet states as a function of the hydrogen bond length: ⟶, exciplex emission.

The fact that the emission can only be observed in the region with a mole fraction of H_2O greater than 0.5 could mean that the hydrogen-bonded $\pi\pi^*$ singlet state lies below the $n\pi^*$ singlet state only in this region. No emission of this kind has been observed in other hydrogen bonding solvents such as TFE and 1,1,1,3,3,3-hexafluoropropanol-2 (HFP-2), despite the fact that the excited molecules are thought to be fully hydrogen bonded in both these solvents. The absence of the emission might mean that either the lowest singlet state is not of $\pi\pi^*$ type or the intersystem crossing rate $S_1 \rightarrow T_0$ has increased. The latter possibility seems implausible in view of the results of the picosecond experiments. The reason why $n\pi^*$ and $\pi\pi^*$ singlet states do not interchange on hydrogen bonding with TFE or HFP-2 might be that a combined action of a strong hydrogen bond and a high polarity of the solvent is needed to invert the two states.

3.4. Photochemical relaxation of electronically excited 3,5 dinitroanisole

We have to rule out photochemical reactions in the mechanism of the fast excited state decay of 3,5-DINA. The type of photochemical processes that might lead to a fast deactivation of the excited state of the nitroanisoles are photoionization, hydrogen abstraction and photodissociation or photoisomerization. Photo-ionization of 3,5-DINA in H_2O does not occur. This must be concluded because neither the absorption spectrum of the ion nor the spectrum of the solvated electron is observed after excitation of 3,5-DINA [6]. If photo-ionization in H_2O is improbable, then it will be even less probable in solvents with a lower polarity. It is known that hydrogen abstraction by nitro aromatic compounds can occur. For some nitro aromatic compounds, such as 4-nitroanisole, reversible hydrogen abstraction

reactions of the following type have been observed (where Ar and Ar′ denote aryl groups):

$$ArNO_2^* + Ar'OH \longrightarrow ArNO_2H\cdot + Ar'O\cdot$$

$$ArNO_2H\cdot + Ar'O\cdot \longrightarrow ArNO_2 + Ar'OH$$

Such reactions have been detected with chemically induced dynamic nuclear polarization (CIDNP) and occur when a very good hydrogen donor such as 2,6-di-*tert*-butylphenol (DBP) is used. The OH bond dissociation energy of DBP is known to be exceptionally low, namely 333 kJ mol^{-1} [31, 32]. We have tried to observe such reactions for 3,5-DINA in CH_3CN and isopropanol but no photo-induced CIDNP is observed in such solutions. Therefore no hydrogen abstraction by excited 3,5-DINA seems to occur. If hydrogen abstraction occurs the resulting 3,5-DINA H· radical should be observed by its absorption band in the visible region [33]. As we observed no absorption in the visible region after the decay of the triplet state we conclude that hydrogen abstraction is not an important decay channel. Photodissociation has long been held responsible for the absence of any fluorescence with wavelengths shorter than 400 nm. The primary product thought to result from a predissociation process is the $NO_2\cdot$ radical [8]. If photodissociation were to occur it is reasonable to assume that not all the primary products would recombine. Photodissociation experiments on iodobenzene show that recombination in solution is never 100%. In low viscosity solvents recombination efficiency amounts to 75%, whereas in very viscous solvents like hexadecane 5% still do not recombine [34]. Of course the recombination rate depends also on the reactivity of the two radicals. As $NO_2\cdot$ is a stable radical, this recombination efficiency will certainly not be very high, and in solvents such as CH_3CN and CH_2Cl_2 we expect that the recombination efficiency will also not be very high. Therefore if $NO_2\cdot$ is formed, we should have been able to observe it, since the $NO_2\cdot$ absorption has for instance been observed after photolysis of nitromethane, where $NO_2\cdot$ is formed several nanoseconds after the photolysis pulse [35]. We conclude that no $NO_2\cdot$ radicals are formed, because we do not observe any absorption in the visible region [36] after the decay of T_0.

For all the conceivable photochemical processes of 3,5-DINA it can be said that if they occur at all they must be very inefficient in the radiationless decay of excited 3,5-DINA.

3.5. 4-tert-butyl-3,5-dinitroanisole

We have investigated the picosecond transient spectroscopy of B-DINA to look for the effect of strong steric hindrance by the *tert*-butyl group on the relaxation of the excited molecule. There are several ways in which the *tert*-butyl group might influence the radiationless relaxation of 3,5-DINA. The *tert*-butyl group in B-DINA forces the NO_2 groups out of the plane of the benzene ring. This shifts the C—NO_2 torsional oscillation to a higher frequency than in 3,5-DINA. If the torsional mode were to act as a prominent accepting or promoting mode in the electronic relaxation of 3,5-DINA a

very different behaviour in the excited state relaxation of B-DINA is to be expected. Another reason why the excited state relaxation of S_1 of B-DINA might be different from that of 3,5-DINA is that the out-of-plane NO_2 groups may cause mixing of the parent $n\pi^*$ and $\pi\pi^*$ states of 3,5-DINA. However, if the π^* orbital is really localized on the NO_2 groups then the rotation of the NO_2 groups will cause little mixing of the first $n\pi^*$ and $\pi\pi^*$ states.

The crystal structure of B-DINA reveals that the NO_2 groups are rotated 65° around the C—N axis out of the benzene plane and that both C(1) and C(4) are slightly tilted from the plane through the remaining ring carbon atoms. This plane makes an angle of 9° with the C(2)–C(1)–C(6) and the C(3)–C(4)–C(5) planes [37].

As for 3,5-DINA, there is no detectable fluorescence or phosphorescence from B-DINA under any circumstances. The $T_n \leftarrow T_0$ absorption band of B-DINA after excitation with a 353 nm light pulse is shown in Fig. 17. The displayed absorption band has been identified as a $T_n \leftarrow T_0$ absorption band by quenching its intensity with a triplet state quencher such as tetramethyldiazetinedioxide or oxygen.

The triplet state lifetime of B-DINA is given in Table 3 for several solvents. The variation in the lifetime with the solvent chosen resembles the behaviour already encountered for 3,5-DINA. Hydrogen bonding of the triplet state again enhances the lifetime; however, in the polar solvent CH_3CN the lifetime exceeds that of the triplet state of 3,5-DINA.

For solutions in *non*-polar solvents the triplet state absorption of B-DINA could not be observed with our nanosecond spectrometer with 5 ns resolution. However the $T_n \leftarrow T_0$ absorption band mentioned above is seen on a picosecond time scale. This means that the lifetime of T_0 is less than 5 ns in non-polar solvents. The increase in the lifetime τ from 5 ns or less to 85 ns in going from a non-polar solvent to CH_3CN appears to reflect the interchange of $^3n\pi^*$ and $^3\pi\pi^*$ levels owing to the action of the reaction field in CH_3CN. In contrast with 3,5-DINA the lowest triplet state of B-DINA in CH_3CN is of $^3\pi\pi^*$ character. The quantum yield of triplet formation, estimated from $D(t_m)$, increases when non-polar solvents are interchanged with polar solvents. This is consistent with the interchange of levels mentioned above and similar to the behaviour of 3,5-DINA.

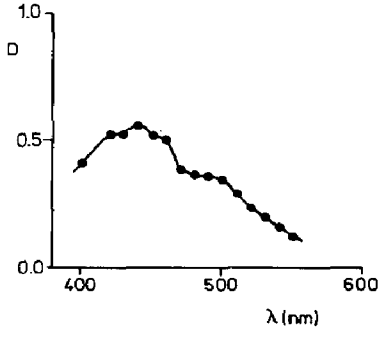

Fig. 17. $T_n \leftarrow T_0$ absorption band of B-DINA in TFE.

TABLE 3

Solvent	*B-DINA*		*3,5-DINA*		*3-NA*
	ϕ_T	τ (ns)	ϕ_T	τ (ns)	τ (ns)
Cyclohexane	0.2[a]	$1 < \tau < 5$	0.2 - 0.4	$1 < \tau < 5$	$1 < \tau < 5$
CH_3CN	0.43	85	0.45	0.8	35
TFE	0.45[a]	3500	0.9	3500	3500

[a] Estimated from $D(t_m)$.

The kinetics of formation of the triplet state of B-DINA after excitation with 353 nm light pulses have been studied in solutions of B-DINA in cyclohexane, CH_3CN and TFE. The measurement of $R(\Delta t)$ on a picosecond time scale has been carried out at 433 nm. The rate constants involved in populating the lowest triplet state and in the decay of the primary excited singlet state have been determined in the same manner as for 3,5-DINA. We have determined the triplet quantum yield required in the analyses for a solution of B-DINA in CH_3CN. The value ϕ_T of 0.43 is used in the simulation and also to transform $D(t_m)$ to ϕ_T for other solvents. The experimental and simulated curves of $R(\Delta t)$ for solutions of B-DINA in CH_3CN and TFE, shown in Fig. 18, coincide exactly. A totally different curve is observed in cyclohexane. The rise time is shorter and the optical density $D(t_m)$ is a factor of 2 lower than in the previous solutions. This is further illustrated by the values in Table 4.

From the simulations we find that the contribution of an $S_n \leftarrow S_1$ absorption to the $R(\Delta t)$ curve is small just as for 3,5-DINA. The ratio ϵ_S/ϵ_T

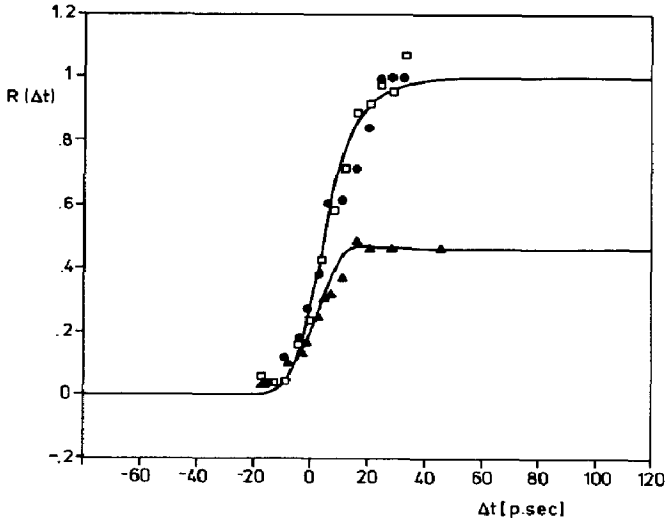

Fig. 18. Growth of transient $T_n \leftarrow T_0$ absorption of B-DINA in various solvents: □, TFE; ●, CH_3CN; ▲, cyclohexane.

TABLE 4

Rate constants for 4-*tert*-butyl-3,5-dinitroanisole

Solvent	ϕ_T	ϵ_S/ϵ_T	k_1 ($\times 10^{10}$ s^{-1})	k_2 ($\times 10^{10}$ s^{-1})	k_7 ($\times 10^9$ s^{-1})
CH_3CN	0.43	0.0	5.3 - 7.5	4.0 - 5.0	1 - 0.2
	0.43	0.1	5.3	4.0	1 - 0.2
	0.43	0.3	n	n	1 - 0.2
Cyclohexane	0.2 [a]	0.0	8 - 12	2 - 4	1 - 0.2
	0.2	0.1	5	1.25	1 - 0.2
	0.2	0.2	n	n	1 - 0.2
TFE	0.45 [a]	0.0	8.0	6.0	< 0.001
	0.45	0.2	4.0	3.0	< 0.001

n, no good fit obtained.
[a] Estimated from $D(t_m)$.

in non-polar solutions may lie between 0 and 0.1 and in polar solutions between 0 and 0.3. Probably in all solutions $\epsilon_S/\epsilon_T \leqslant 0.1$. If we compare the rate constants in Table 4 at equal ratios of ϵ_S/ϵ_T then it is observed that k_1 is larger than k_2 in cyclohexane solution and approximately equal to k_2 in polar solutions. The rate constant k_2 does not seem to vary with change in polarity. The differences with 3,5-DINA are that in hydrogen bonding solvents k_1 does not become much smaller than k_2 and that in polar solutions the lowest triplet state of B-DINA is already a $^3\pi\pi^*$ state. The fact that ϕ_T does not seem to increase, on going from CH_3CN to TFE as solvent, is difficult to understand. We observe clearly a solvent effect on the triplet lifetime, and therefore we assume that the $^3\pi\pi^*$ state can form a long-lived hydrogen bond with the solvent. An explanation might be that hydrogen bond formation here cannot compete with S_i relaxation, owing to a slower hydrogen bonding reaction. A reason for a slower hydrogen bonding reaction with S_i may be the steric hindrance of the *tert*-butyl group or reduced polarity of the charge transfer state, which makes the NO_2 group less accessible or reactive for hydrogen bond formation. Another possibility might be that there is a relaxation path of S_1 present, which does not exist in 3,5-DINA and remains operative after hydrogen bonding. Such a relaxation mechanism could be a photochemical deactivation of S_1 via an intramolecular reversible hydrogen abstraction as suggested for other *tert*-butyl nitro aromatics [38]. Indeed some photochemical reactions are observed for B-DINA in CH_3CN. However, the quantum yield of such reactions is very low, which seems to exclude photochemical deactivation as a main decay channel.

Although a number of uncertainties still remain, we conclude that the introduction of the *tert*-butyl group between the two NO_2 groups does not change the relaxation behaviour of 3,5-DINA dramatically. The introduction of the *tert*-butyl group does not appreciably slow down the very efficient $S_1 \rightarrow S_0$ and $T_0 \rightarrow S_0$ radiationless decay in non-polar solvents.

3.6. 3-nitroanisole

The relaxation of excited 3-NA resembles the relaxation of 3,5-DINA and B-DINA. Again a $T_n \leftarrow T_0$ absorption is observed in polar and hydrogen bonding solvents (λ_{max} = 435 nm) as is shown in Fig. 19. In non-polar solvents no $T_n \leftarrow T_0$ absorption is observed on a nanosecond time scale.

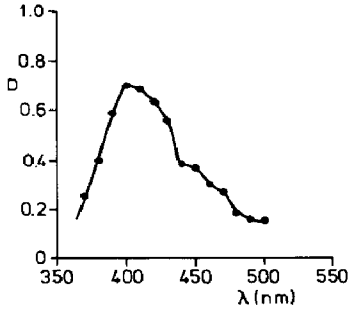

Fig. 19. $T_n \leftarrow T_0$ absorption spectrum of 3-NA in TFE observed on a nanosecond time scale.

TABLE 5

Rate constants for 3-nitroanisole

Solvent	ϕ_T	ϵ_S/ϵ_T	k_1 ($\times 10^{10}$ s^{-1})	k_2 ($\times 10^{10}$ s^{-1})	k_7 ($\times 10^9$ s^{-1})
CH_3CN	1.0[a]	0.0	0	15	0.033
		0.5	0	12	0.033
		1	n	n	
TFE	1.0[a]	0.0	0	15	< 0.001
		0.5	0	12	< 0.001

n, no good fit.
[a] Estimate.

The picosecond relaxation of 3-NA has been studied in two solvents only, CH_3CN and TFE. As in the previous case of B-DINA the curves $R(\Delta t)$ in CH_3CN and TFE are exactly coincident. In the simulation we chose ϕ_T = 1.0, because $D(t_m)_{DINA} \approx D(t_m)_{3\text{-NA}}$ in TFE. (From photochemical experiments we know that $\phi_T > 0.5$ [39].) The rate constants thus obtained are given in Table 5, and the simulated curve together with the experimental results are shown in Fig. 20.

The rise time of the $R(\Delta t)$ curves is very short; therefore the values of k_1 and k_2 given are lower limits. Without a more precise knowledge of ϕ_T it is not possible to calculate k_1 and k_2. However, in view of the previous results it is probable that $k_1 > k_2$ in non-polar solvents, whereas in polar solvents it is expected that the internal conversion process will become slower while the rate constant for intersystem crossing will remain the same.

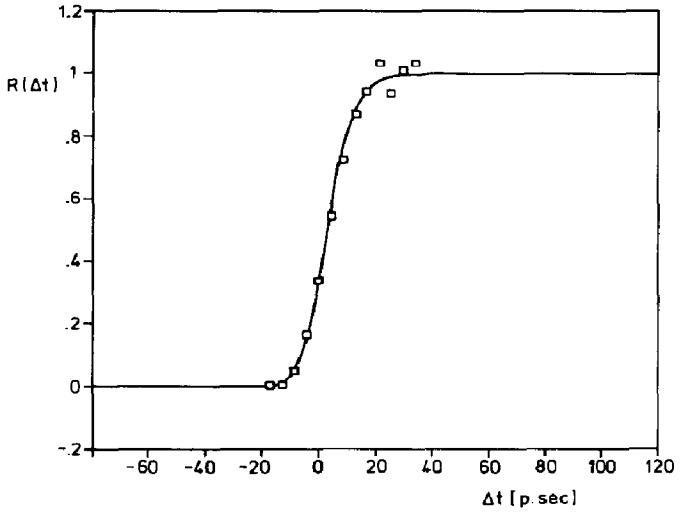

Fig. 20. Growth of the transient $T_n \leftarrow T_0$ absorption of 3-NA in CH_3CN. A similar curve is observed for 3-NA in TFE.

3.7. The cause of ultrafast radiationless decay of electronically excited nitroanisoles

Two main conclusions of the present work need an explanation, namely the high rates of $S_i \rightarrow S_0$ internal conversion and $T_0 \rightarrow S_0$ intersystem crossing, observed in 3,5-DINA, 3-NA and B-DINA in non-hydrogen-bonding solvents, and the effect of hydrogen bonding on these relaxation rates.

Often the radiationless decay of aromatic hydrocarbons is adequately described by a near-exponential energy gap law [40]. It relies on the assumption that only the highest frequency vibrational mode accepts the electronic excitation energy. In aromatic hydrocarbons the C—H stretching vibrational mode then acts as the efficient accepting mode. Its importance is clearly demonstrated by the effect of deuteration on the rates of electronic relaxation [40 - 42]. However, for the nitroanisoles we determined rate constants for radiationless decay in non-polar solvents that are many orders of magnitude larger than can be explained by the energy gap law. We obtained $10^{11}\ s^{-1} \leqslant k_{S_i \rightarrow S_0} \leqslant 10^{12}\ s^{-1}$ and $k_{T_0 \rightarrow S_0} \approx 10^9\ s^{-1}$. Aza aromatic and nitro aromatic compounds are the only other types of molecules for which internal conversion rates of these orders of magnitude have been reported while having $S_1 \rightarrow S_0$ energy gaps larger than 2.5 eV [5, 40, 43 - 47]. A rate constant as high as $10^9\ s^{-1}$ for $T_0 \rightarrow S_0$ intersystem crossing has not been measured earlier. Only in the case of nitrobenzene has the triplet lifetime been estimated to be of the order of 1 ns [21].

Let us refer to the electronic energy level scheme in Fig. 1. The first excited singlet state S_1 is an $n\pi_1^*$ state in which an electron from the NO_2 groups is excited to the π_1^* molecular orbital which is mainly localized on the NO_2 groups. The dipole moment of this state is comparable with that of the ground state. A CNDO/S–CI calculation predicts two nearly degenerate $n\pi_1^*$ states which have very similar electronic structures. For simplicity we

consider the two $n\pi_1^*$ states together as S_1. The second excited singlet state S_2 is a charge transfer state which has a large contribution from the singly excited configuration with an electron from the anisole moiety of the molecule excited to the π_1^* orbital. This excitation leads to a large increase in the electron density on the NO_2 groups and therefore to a large increase in dipole moment. Owing to the charge localization, the 3,5-DINA molecule in its S_2 state will be capable of forming a hydrogen bond between one of the NO_2 groups and a solvent molecule, *e.g.* H_2O. This is in contrast with the $n\pi_1^*$ state which will have less tendency to form hydrogen bonds than the ground state. Therefore these levels should shift in opposite directions in a hydrogen bonding solvent.

The S_2–S_1 energy gap is estimated to vary between about 4000 and 0 cm^{-1}, depending on the solvent polarity. In hydrogen bonding solvents the S_2–S_1 energy gap is thus expected to become very small and the S_1 and S_2 states may even reverse their order. The corresponding $^3n\pi_1^*$ and $^3\pi\pi_1^*$ states, T_0 and T_1, are thought to lie in even closer proximity. As discussed before there are three reasons to identify the lowest triplet state of 3,5-DINA in non-hydrogen-bonding solvents as a $^3n\pi_1^*$ state. First, there is a great similarity between the triplet lifetime of nitrobenzene and of 3,5-DINA. The lowest triplet state of nitrobenzene has been identified on chemical grounds as a $^3n\pi^*$ state [21, 22]. Secondly, we concluded from the picosecond experiments in CH_3CN–H_2O mixtures that 3,5-DINA in its lowest non-hydrogen-bonded triplet state has a low reactivity towards hydrogen bonding, which is typical for a $^3n\pi_1^*$ state. The third reason is the large decrease in the $T_0 \rightarrow S_0$ intersystem crossing rate when going from non-hydrogen-bonding to hydrogen bonding solvents. In the hydrogen bonding solvents the lowest triplet state of 3,5-DINA has been identified as a $^3\pi\pi_1^*$ state, and an interchange of the $^3n\pi_1^*$ and $^3\pi\pi_1^*$ states may explain the observed large difference in lifetime. We concluded that whenever the decay processes $S_i \rightarrow S_0$ and $T_0 \rightarrow S_0$ are very fast, they originate from singlet and triplet states which have $n\pi^*$ character.

To explain the high rates of internal conversion and intersystem crossing in nitrogen heterocyclic aromatics a model was introduced which allows vibronic coupling between the first two crude Born–Oppenheimer excited singlet states [48]. The vibronic coupling leads to a distortion of the potential energy surfaces of these excited states, which leads to a strong enhancement of the $S_1 \rightarrow S_0$ and $T_0 \rightarrow S_0$ radiationless transition rates. These model calculations also reveal that the $S_1 \rightarrow T_0$ intersystem crossing rate is hardly influenced by the coupling of the two states. It has been shown that the low frequency mode which couples the two zero-order states may be an efficient accepting mode in the radiationless transitions [49, 50]. For sufficiently small energy gaps and large vibronic interaction strength such a mode may even become the dominant accepting mode. These aspects are referred to as the proximity effect. It must be noted, however, that there is no physical effect involved, but an improvement on an inadequate theoretical description.

Because there are closely spaced $n\pi^*$ and $\pi\pi^*$ excited states in the nitroanisoles it is useful to examine whether the high rates of radiationless decay can be explained by the proximity effect. The proximity effect cannot be the main reason for the fast excited state decay in nitroanisoles because of what follows. We encountered two cases in which $n\pi^*$ and $\pi\pi^*$ states are close together. In CH_3CN as solvent, the $^3n\pi_1^*$ is slightly below the $^3\pi\pi_1^*$ state, whereas in H_2O the $^3\pi\pi_1^*$ is probably not far below the $^3n\pi_1^*$ state. As far as the proximity effect is concerned there should not be much difference between the decay rates in the two cases. However, experimentally the ratio of the two rate constants is at least 10^3. The proximity effect would also predict a decrease in the $S_1 \rightarrow S_0$ relaxation rate of 3,5-DINA in going from polar to non-polar solvents because the S_1–S_2 energy gap is then becoming larger. However, the reverse effect is observed.

We suggest that the fast $S_1 \rightarrow S_0$ and $T_0 \rightarrow S_0$ decay from the $n\pi_1^*$ states is caused by a deformation of the NO_2 group, arising on excitation of the nitroanisole to the $n\pi_1^*$ state. Since the $n\pi_1^*$ excitation is highly localized on the NO_2 groups a deformation and displacement of the $n\pi_1^*$ potential energy surface with respect to the ground state are expected. The magnitude of the displacement and distortion in the NO_2 group may be inferred from a spectroscopic and quantum chemical study of the nitrite anion in solution [51]. In the nitrite anion $n\pi^*$ transitions similar to those observed in nitro aromatic compounds are possible. From calculations of the band shape and position it is concluded that the O—N—O angle decreases by 10° on excitation to the $n\pi^*$ state and that the frequencies of the stretching and bending vibrations decrease by about 30% [51]. This means that the potential energy surface of the $n\pi^*$ state is strongly distorted and displaced compared with the ground state. In Fig. 21 it is shown how such a large deformation, along the O—N—O bending coordinate, may lead to strong non-adiabatic coupling and large Franck–Condon factors for internal conversion for the $n\pi_1^*$ state.

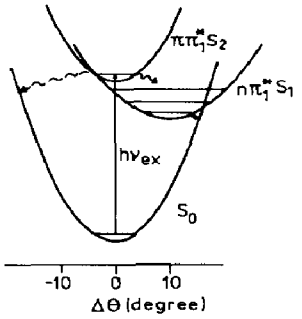

Fig. 21. Conceivable potential energy surfaces along the O—N—O bending coordinate of the NO_2 group. A tentative relaxation path $\pi\pi_1^* \rightarrow n\pi_1^* \rightarrow S_0$ is indicated.

No deuterium effect has been found in the decay of the $^1n\pi_1^*$ and $^3n\pi_1^*$ states of 3,5-DINA. This means that the C—H vibrations are not important as accepting modes in the decay of these states, which is in accordance with the point of view that the excitation is localized on the NO_2 groups. The C—NO_2

torsional motion may also be ruled out as an efficient accepting mode because we also observe high rates of radiationless relaxation in B-DINA, where this motion is strongly inhibited by the *tert*-butyl group. Therefore the important accepting modes must be other local vibrations of the NO_2 group such as the O—N—O bending and N—O stretching vibrations.

Excitation of 3,5-DINA with 353 nm light populates primarily the $^1\pi\pi_1$ state, because the oscillator strength of the $\pi_1^* \leftarrow \pi$ transition exceeds that of the $\pi_1^* \leftarrow$ n transition by nearly a factor of 10^2. The relaxation of $S_i(\pi\pi_1^*)$ then proceeds via $S_i \rightarrow T_0$ intersystem crossing and internal conversion to S_0 via S_1, in competition with hydrogen bonding between S_i and an H_2O molecule. The above could mean that the internal conversion process $S_2 \rightarrow S_1$ is not as fast as is usual for $S_n \rightarrow S_1$ internal conversion.

The low rate of $S_2 \rightarrow S_1$ relaxation may be explained by the small energy gap between S_2 and S_1. In polar solvents this energy gap is estimated to be smaller than 2000 cm^{-1}, which may result in a low density of energy dissipating states in S_1 and consequently in a low rate of $S_2 \rightarrow S_1$ relaxation [52]. Such an effect has for instance been observed in isoquinoline where the S_2 and S_1 states are separated by an energy gap of about 1000 cm^{-1} and where the rate constant for $S_2 \rightarrow S_1$ relaxation was estimated to be 10^{10} s^{-1} [52]. This value corresponds in order of magnitude to the value of k_1 of 3,5-DINA in CH_3CN. The observed increase in k_1 in going from CH_3CN to less polar solvents such as CH_2Cl_2 might then be rationalized as follows. In non-polar solvents the energy gap ΔE between S_2 and S_1 is larger than in polar solvents. An increase in ΔE is accompanied by a higher density of energy dissipating states and thus by an increase in k_1.

We conclude that electronically excited nitroanisoles exhibit unusually fast radiationless decay, when S_1 and T_0 are $n\pi^*$ states with the excitation localized on the NO_2 groups. Then the $n\pi^*$ potential energy surfaces are distorted and displaced to a larger extent relative to S_0 than predicted by pseudo Jahn–Teller corrections, *i.e.* the proximity effect. Hydrogen bond formation may take place between the $^1\pi\pi^*$ charge transfer state and the solvent molecules. When the solvent contains only a minor hydrogen bonding component, the reaction is first order and limited by diffusion. The reaction between the excited $^1\pi\pi_1^*$ state and one H_2O molecule leads to a charge localization in the excited 3,5-DINA molecule and to an inversion of $^3\pi\pi^*$ and $^3n\pi^*$. Hydrogen bonding may also lead to an inversion of $^1\pi\pi^*$ and $^1n\pi^*$ states. The relaxation of $^1\pi\pi^*$ and $^3\pi\pi^*$ states to the ground state is much slower than that of the $n\pi^*$ states.

In Table 6 some characteristic data on nitro aromatics are gathered. If we compare the rate constants, quantum yields etc., the following general conclusions on the decay of the nitro aromatic compounds may be drawn. The $n\pi^*$ states are not very sensitive for the type of aromatic systems to which the NO_2 group is attached, because of the localized excitation character of this state. The energy level of the $^3n\pi^*$ state is estimated to lie about 20 000 cm^{-1} above S_0. The $\pi\pi^*$ charge transfer state, however, is strongly dependent on the type of aromatic system to which the NO_2 group

TABLE 6

	ϕ_F	ϕ_T	ϕ_P	k_1 [a] (s^{-1})	k_2 (s^{-1})	k_7 (s^{-1})
Nitrobenzene[b]	$<10^{-4}$	0.6	$<10^{-4}$	—	—	10^9
3,5-DINA[c]	$<10^{-4}$	0.4	$<10^{-4}$	1×10^{11}	8×10^{10}	1.2×10^9
3,5-DINA[d]	$\leq10^{-4}$	0.9	$<10^{-4}$	$<10^{10}$	8×10^{10}	$<10^6$
2-nitronaphthalene[e]	$\leq10^{-4}$	0.83	0.26	5×10^{10}	6×10^{10}	17
3-nitroaniline[e]	0.135	—	—			

[a] Rate constants as defined in Fig. 14.
[b] Nitrobenzene has long been thought to show a very weak phosphorescence which is probably spurious [53, 54].
[c] In CH_3CN solution.
[d] In aqueous solution.
[e] From refs. 10, 44, 45 and 53.

is attached. The $\pi\pi^*$ states decrease in energy with increasing electron-donating power or lower ionization potential of the aromatic system. Therefore the $\pi\pi^*$ state decreases in energy in the order nitrobenzene, 3-NA, 2-nitronaphthalene and 3-nitroaniline. As a consequence the triplet state of nitrobenzene is always of $n\pi^*$ character. In the nitroanisoles it may be either $n\pi^*$ or $\pi\pi^*$, depending on the solvent. In nitronaphthalene and nitroaniline the triplet is always of $\pi\pi^*$ character. If the lowest triplet is of $\pi\pi^*$ character, then it may become phosphorescent. Intersystem crossing is always very fast, if $^1n\pi^* \rightarrow {}^3\pi\pi^*$ and/or $^1\pi\pi^* \rightarrow {}^3n\pi^*$ processes are possible. In 3-nitroaniline the lowest $^1\pi\pi^*$ singlet state is lower in energy than the $^3n\pi^*$ state and intersystem crossing is much less efficient. Therefore we observe fluorescence in this case. Whether fluorescence appears in nitro aromatic compounds is determined by the energy level of the $^3n\pi^*$ state relative to the $^1\pi\pi^*$ state, and not by photodissociation. Despite the very high rate of intersystem crossing the quantum yield for triplet formation is not unity in most nitro aromatic compounds. As in the nitroanisoles this is probably caused by a very fast internal conversion process, originating from the $^1n\pi^*$ state. Whenever a lowest triplet state is observed with a lifetime of not more than about 10^{-9} s, it must be a $^3n\pi^*$ state with localized excitation.

A recent formulation of the theory of radiationless electronic transitions in molecules clearly shows where promoting modes, displacement and detuning of accepting modes and temperature enter the expression for the radiationless decay rate constant [55, 56]. The theory is restricted by the following conditions. After excitation, vibrational relaxation is much faster than electronic relaxation and thus a thermal equilibrium population over the initial states with vibrational quantum number v' in the electronic state Ψ_b exists. The Condon approximation is sufficiently adequate.

The frequency shift and displacement of oscillators may be neglected in promoting mode factors. Molecular vibrations are treated as harmonic oscillations of the normal coordinates Q_i. The molecular states are described in the

adiabatic approximation $\Psi_{kv} = \Phi_k \theta_{kv}$, with Φ_k the electronic wavefunction and θ_{kv} the vibrational wavefunction in the kth electronic state. The probability $W(\mathrm{b} \rightarrow \mathrm{a})$ for a transition from electronic state Φ_b to Φ_a is given by

$$W(\mathrm{b} \rightarrow \mathrm{a}) = \frac{1}{2} \sum_i |R_i(\mathrm{ab})|^2 \frac{\omega_i'}{2\hbar} \left[\frac{1}{2} \left\{ \coth\left(\frac{\hbar\omega_i'}{2kT} \right) + 1 \right\} f_i(\omega_{\mathrm{ab}} + \omega_i') + \right.$$
$$\left. + \frac{1}{2} \left\{ \coth\left(\frac{\hbar\omega_i'}{2kT} \right) - 1 \right\} f_i(\omega_{\mathrm{ab}} - \omega_i') \right] \tag{29}$$

with the promoting mode factor $R_i(\mathrm{ab})$ taken as

$$R_i(\mathrm{ab}) = -\hbar^2 \left\langle \Phi_\mathrm{a} \left| \frac{\partial}{\partial Q_i} \right| \Phi_\mathrm{b} \right\rangle \tag{30}$$

Detuning and displacement parameters of normal modes are defined as

$$\rho_j = \frac{\omega_j' - \omega_j''}{\omega_j''} \tag{31}$$

$$\Delta_j^2 = \left(\frac{\omega_j'}{\hbar} \right)^{1/2} (Q_j'' - Q_j')^2 \tag{32}$$

The phonon coupling strength $\hat{S}$ is defined by

$$\hat{S} = \sum_j \frac{1}{2} \Delta_j^2 \coth\left(\frac{\hbar\omega_j}{2kT} \right) \tag{33}$$

The functions f_i evaluated at $T = 0$ are expressed as

$$f_i(\omega_{\mathrm{ab}} \pm \omega_i') = 2\pi \exp(-\hat{S}_0) \sum_{v_1} \cdots \sum_{v_\mathrm{N}} \prod_j \frac{1}{v_j!} \left(\frac{\Delta_j^2}{2} \right)^{v_j} \delta(\omega_{\mathrm{ab}}' \pm \omega_i' + \sum_j v_j \omega_j') \tag{34}$$

Here

$$\hat{S}_0 = \hat{S}(T = 0) = \sum_j \frac{1}{2} \Delta_j^2 \tag{35}$$

and

$$\omega_{\mathrm{ab}}' = \omega_{\mathrm{ab}} - \frac{1}{2} \sum_j \rho_j \omega_j' \tag{36}$$

at $T = 0$. To obtain a manageable expression for the temperature dependence of $W(\mathrm{b} \rightarrow \mathrm{a})$, the frequencies and displacements of all accepting modes are given values $\bar{\omega}'$ and $\bar{\Delta}_j^2$ respectively, which represent averages of the actual values for the different modes. This is not a serious defect in the treatment of an excitation localized on an NO_2 group, because only the local N—O stretch and NO_2 bending vibrations are important. By defining

$$T^* = \frac{kT}{\hbar\bar{\omega}'}$$

$$W^*(\mathrm{b} \rightarrow \mathrm{a}, T) = \frac{W(\mathrm{b} \rightarrow \mathrm{a}, T)}{W(\mathrm{b} \rightarrow \mathrm{a}, 0)} \tag{37}$$

and

$$\omega_{\mathrm{ba}}{}'^* = \frac{\omega_{\mathrm{ab}}{}'}{\bar{\omega}'}$$

the temperature dependence for low temperatures, *i.e.* $kT < \hbar\bar{\omega}'$, becomes

$$W^*(\mathrm{b} \rightarrow \mathrm{a}, T) = 1 + \exp\left(-\frac{1}{T}\right)\left\{\omega_{\mathrm{ba}}{}'^* - 2\hat{S}_0 + \frac{\hat{S}_0{}^2}{\omega_{\mathrm{ba}}{}'^*} + \frac{\hat{S}_0{}^2}{\omega_{\mathrm{ba}}{}'^*(\omega_{\mathrm{ba}}{}'^* + 1)}\right\} \tag{38}$$

Below a certain temperature limit T_c the effect of temperature is small. The threshold temperature $T_c{}^*$ is

$$T_c{}^* = \frac{1}{\ln\{\omega_{\mathrm{ba}}{}'^* - 2\hat{S}_0 + (\hat{S}_0{}^2/\omega_{\mathrm{ba}}{}'^*) + \hat{S}_0{}^2/\omega_{\mathrm{ba}}{}'^*(\omega_{\mathrm{ba}}{}'^* + 1)\}} \tag{39}$$

The behaviour of $W^*(\mathrm{b} \rightarrow \mathrm{a}, T^*)$ has been studied for various choices of $\hat{S}_0$ and $\omega_{\mathrm{ba}}{}'^*$ [56]. For a fixed coupling strength $\hat{S}_0$ the temperature effect increases with increasing energy gap $\omega_{\mathrm{ba}}{}'^*$, and for a fixed energy the temperature effect increases with decreasing $\hat{S}_0$. The theory shows that large displacements in the local NO_2 vibrational modes are to be associated with a strong phonon coupling $\hat{S}_0$. Similarly large phonon coupling strengths may be expected for other locally excited small chromophores, *e.g.* keto groups. The much faster radiationless decay of the local excitation on NO_2 groups must therefore be due to a further amplification of the transition probability by the promoting mode factors $R_i(\mathrm{ab})$. The electron distribution in the $n\pi^*$ states, with excitation localized on the NO_2 group, is expected to be highly modulated by vibrations which modulate the overlap of lone pair orbitals centred on different oxygen atoms, *e.g.* NO_2 bending and N—O stretching modes. Then the derivative of the electronic wavefunction with respect to the corresponding normal coordinates must be large. The theory also allows the absence of a temperature effect in the radiationless decay of the nitroanisole to be associated with the strong phonon coupling $\hat{S}_0$.

4. Results and discussion: decay of hydrogen-bonded triplet state of nitroanisoles in relation to the electronic structure of their excited states and the properties of the solvent

4.1. Electronic structure of the nitroanisoles

4.1.1. UV absorption spectra

The gas phase UV absorption spectra of nitrobenzene and some of its derivatives are given in a number of recent publications [57, 58]. In Fig. 22 the gas phase spectrum of 3,5-DINA is shown together with some spectra of 3,5-DINA in solution. The spectra are characterized by three intense absorption bands around 200, 230 and 310 nm. A weak broad band around 360 nm can only be distinguished clearly in the gas phase spectrum. The assignment of the absorption bands of nitrobenzene and some of its derivatives has been the subject of discussion in several publications [59 - 66]. In most cases only the strong absorption bands were considered. These bands are ascribed to $\pi^* \leftarrow \pi$ transitions. Much less attention was given to the weak absorption bands, which are most probably caused by $\pi^* \leftarrow$ n transitions, as we may infer from their low oscillator strength and from their polarization [59 - 64]. Our attention will be focused mainly on the lowest excited states because these determine the rate of relaxation of the primary excited state to the ground state. Figure 22 reveals a large bathochromic shift in going from the gas phase to a solution and from non-polar to polar solutions. From these solvent-induced shifts in the absorption bands and also from electro-optical measurements it is possible to deduce the changes in electric dipole moment which occur on excitation [67, 68]. In this way the dipole moments of several $\pi\pi^*$ excited states of nitrobenzene, 3-NA and 3,5-DINA have been obtained [39, 69]. All these molecules have considerably larger dipole moments in their $\pi\pi^*$ excited states than in the ground state. For instance, 3,5-DINA has dipole moments of 8.5 debyes and 4.0 debyes in the

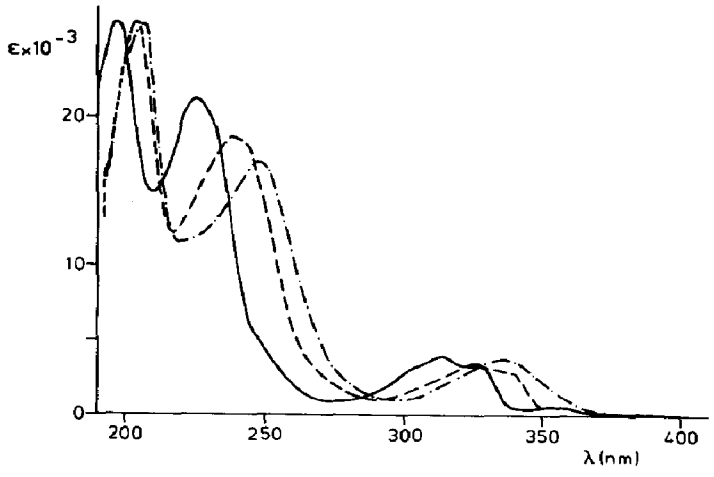

Fig. 22. UV absorption spectra of 3,5-DINA: ——, gas phase spectrum; — — —, in cyclohexane; —· —, in CH_3CN.

first excited $^1\pi\pi^*$ state and ground state respectively [20]. The large increase in dipole moment has been related to transfer of charge from the benzene moiety to the NO_2 group(s) [60].

Because the weak $\pi^* \leftarrow$ n absorption bands are severely overlapped by much more intense $\pi^* \leftarrow \pi$ absorption bands it is hardly possible to observe any solvent shift in the weak absorption bands. The solvent-induced shift of the $\pi^* \leftarrow$ n band in nitrobenzene has therefore been a source of confusion, but finally it has been concluded that no red shift occurs with increasing solvent polarity [58]. A small blue shift might be involved as for 1,3,5-trinitrobenzene. Consequently it has been concluded that the dipole moment of the $n\pi^*$ state of nitrobenzene is equal to or somewhat smaller than that of the ground state [58]. The same appears to hold for the $n\pi^*$ states of 3,5-DINA and 3-NA from the solvent effect on the first weak absorption band.

4.1.2. Complete neglect of differential overlap/spectroscopic–configuration interaction quantum chemical calculations

Semiempirical quantum chemical methods such as the Nagakura–Tanaka [60] charge transfer model and the Pariser–Parr–Pople molecular orbital (MO) [59] method have been applied to nitro aromatic systems. These methods do not take $n\pi^*$ states into account. Since several $n\pi^*$ states are expected among the lowest excited states of the nitro aromatic compounds we applied the CNDO/S–CI method with standard parametrization [70] to find the ordering of energy levels and the charge distributions of the lower excited states [71]. The total wavefunction for the nth excited state will be denoted as

$$\Phi_n = \sum_i C_{ni}\phi_i \tag{40}$$

Here ϕ_i represents a single configuration with an electron promoted from ground state orbital ψ_k to virtual orbital ψ_l, expressed as $\psi_l \leftarrow \psi_k$. The highest π self-consistent field (SCF) MO occupied in the ground state will be indicated as π_0 and the lower-lying orbitals as π_{-1}, π_{-2} ..., in order of decreasing energy; lone pair orbitals are represented in the same way as n_0, n_{-1} .... Virtual π MOs are labelled as π_1^*, π_2^* ..., in order of increasing energy. The linear combination of atomic orbitals expression for an MO ψ_j is written as

$$\psi_j = \sum_k \sum_\alpha C_{jk\alpha}\chi_{k\alpha} \tag{41}$$

where $\chi_{k\alpha}$ represents an atomic orbital on the kth atom. The fractional population P_{jg} contributed by a molecular fragment g to MO ψ_j is given by

$$P_{jg} = \sum_{k \in g} \sum_\alpha C_{jk\alpha}^2 \tag{42}$$

From the value of P_{jg} it may be judged to what extent an orbital ψ_j is localized on fragment g.

4.1.2.1. Nitrobenzene. The configurations ϕ_i which are important for nitrobenzene in the excited state wavefunctions Φ_n are given in Table 7.

TABLE 7

Truncated wavefunctions of nitrobenzene

$^1\Phi_1 = 0.888(\pi_1^* \leftarrow n_0) + 0.403(\pi_3^* \leftarrow n_0) + \ldots$
$^1\Phi_2 = -0.888(\pi_1^* \leftarrow n_{-1}) - 0.403(\pi_3^* \leftarrow n_{-1}) + \ldots$
$^1\Phi_3 = 0.825(\pi_1^* \leftarrow \pi_0) - 0.474(\pi_2^* \leftarrow \pi_{-1}) + \ldots$
$^1\Phi_4 = -0.977(\pi_1^* \leftarrow \pi_{-1}) + \ldots$
$^3\Phi_1 = 0.902(\pi_1^* \leftarrow \pi_{-2}) + \ldots$
$^3\Phi_2 = 0.888(\pi_1^* \leftarrow n_0) - 0.403(\pi_3^* \leftarrow n_0) + \ldots \approx {}^1\Phi_1$

The orbital population $P_g(\psi)$ contributed by the NO_2 group is given in Table 8 and shows that most of the population due to n_0, n_{-1} and π_1^* is localized on the NO_2 group, whereas π_0 is mainly localized on the phenyl ring. The predicted transition energies, oscillator strengths and dipole moments given in Table 9 are in good agreement with the experimental values and other CNDO/S–CI calculations [62]. The calculated dipole moments μ_g and μ_e of the ground and excited states are too large. This has also been observed for other CNDO calculations [72]. The ratio $R = \mu_e/\mu_g$, however, corresponds to experiment ($R_{exp} = 2.4$; $R_{calc} = 2.6$).

TABLE 8

Localization of the molecular orbitals of nitrobenzene

	n_0	n_{-1}	π_3^*	π_2^*	π_1^*	π_0	π_{-1}	π_{-2}
P_{NO_2}	0.82	0.91	0.28	0.00	0.70	0.05	0.00	1.00

The first two excited states both have $n\pi^*$ character and can be considered as local excitations of the NO_2 group. Excitation to $^1\Phi_1$ causes a decrease in electron density on the oxygen atoms (0.17 electron per oxygen atom) and a small increase in electron density on the phenyl ring (0.18 electron). Consequently the dipole moment in $^1\Phi_1$ is slightly lower than that in the ground state. This reduction in electron density on the oxygen atoms attenuates their tendency to form hydrogen bonds [70, 73]. Excitation to $^1\Phi_2$ involves a similar migration of electron charge from the NO_2 group to the phenyl ring as for $^1\Phi_1$.

We attribute the observed weak absorption band around 360 nm (3.4 eV) in the gas phase spectrum to the transition from $^1\Phi_0$ to $^1\Phi_1$. This is in agreement with the low oscillator strength, the solvent-induced band shift and the polarization determined for this band [61].

The CNDO/S–CI calculation predicts a value of 0.42 eV for the energy gap between $^1\Phi_1$ and $^1\Phi_2$. Other CNDO calculations also predict such a small

TABLE 9

Experimental[a] and calculated properties of nitrobenzene

	Symmetry	*E* (eV)		*f*		*μ* (debyes)		*Polarization*[b]	
		Calculated	*Experimental*	*Calculated*	*Experimental*	*Calculated*	*Experimental*	*Calculated*	*Experimental*
$^1\Phi_i$									
0	A_1	—	—	—	—	5.9	4.22		
1	B_1	2.88	≈3.4	10^{-4}	3×10^{-3}	5.4		*x*	*z*
2	A_2	3.30		0		4.4			
3	B_2	4.55	4.38	0.025	0.01	9.9		*y*	*x* or *y*
4	A_1	4.96	5.11	0.22	0.17	15.3	10	*z*	*z*
5	B_2	5.59		0.015		15.5		*y*	
6	A_1	6.13	6.42	0.42	0.38	7.0		*z*	
$^3\Phi_i$									
1	B_2	1.92							
2	B_1	2.88	⩾2.6						

[a] Experimental values from refs. 1, 3 and 13.

[b] *x* axis perpendicular to the molecular plane; *z* axis coincides with the C_2 axis.

energy gap [63 - 66]. However, we think that this energy gap will be around 0.7 eV, which places $^1\Phi_2$ higher above $^1\Phi_1$. This larger energy gap will be explained later.

The state $^1\Phi_3$ consists mainly of the configuration $\pi_1^* \leftarrow \pi_0$ with an admixture of $\pi_2^* \leftarrow \pi_{-1}$. The first configuration is a charge transfer configuration in which electronic charge migrates from the phenyl ring to the NO_2 group. The second configuration is a locally excited configuration of the phenyl ring. The transition from $^1\Phi_0$ to $^1\Phi_3$, regarding transition energy, polarization and oscillator strength, corresponds to the band at 283 nm (4.38 eV) in the gas phase spectrum.

The state $^1\Phi_4$ mainly consists of the pure charge transfer configuration $\pi_1^* \leftarrow \pi_{-1}$. In this state even more electron density migrates to the NO_2 group than in $^1\Phi_3$ and the dipole moment of this state is very large. The energy, oscillator strength, polarization and large dipole moment agree with the assignment of the 5.11 eV absorption to the $^1\Phi_4 \leftarrow {}^1\Phi_0$ transition. Just as a decrease in electron density leads to a lower tendency towards hydrogen bonding, a large increase in electron density on the oxygen atoms leads to an increase in tendency for hydrogen bonding [70, 73]. The increase in electron density in Φ_4 amounts to 0.16 electron on each of the two oxygens and 0.29 electron on the nitrogen atom.

The CNDO/S–CI procedure proves inadequate for the description of the triplet states. It results in a vanishing separation between $^1n\pi^*$ and $^3n\pi^*$ states with the same electron configuration and therefore does not provide any useful information on the location of $^3n\pi^*$ states relative to $^3\pi\pi^*$ states. Identification of the nature of the lowest triplet state has to rely on experimental data. As already noted, nitrobenzene is believed to have a $^3n\pi^*$ state as the lowest triplet state. The energy level S_1 estimated from solution spectra lies around 3.30 eV. The energy level E_{T_0} of T_0 estimated from quenching experiments is 2.6 eV or more. If S_1 and T_0 have the same electron configuration then a singlet–triplet splitting of 0.7 eV or less might seem rather large for $n\pi^*$ states. This large energy gap seems less surprising, however, if we take into account that both the n_0 and π_1^* orbitals are highly localized on the oxygen atoms of the NO_2 group [74]. The CNDO/S–CI calculation, in contrast, predicts a $^3\pi\pi^*$ state as the lowest triplet state of nitrobenzene which involves a local $\pi^* \leftarrow \pi$ excitation of the NO_2 group. The corresponding singlet state lies at 6.66 eV and the calculation thus presents a singlet–triplet splitting of 4.74 eV owing to the very strong localization of this particular excitation. A poor agreement between predicted triplet states and experimental results has also been found for nitroanilines [64].

4.1.2.2. 3-nitroanisoles. The first two excited singlet states of 3-NA are again two $n\pi^*$ states similar to those in nitrobenzene as shown in Tables 10 and 11. From the data in Tables 10 and 12 it seems that the excitation to $^1\Phi_1$ and $^1\Phi_2$ is somewhat less localized than in the corresponding cases of nitrobenzene and 3,5-DINA. This stands in contrast with the results of an *ab initio* calculation on 3-nitroaniline which predicts fully localized $n\pi^*$ excita-

TABLE 10

Truncated wavefunctions of 3-nitroanisole

$^1\Phi_1 = -0.666(\pi_1^* \leftarrow n_0) - 0.589(\pi_1^* \leftarrow n_{-1}) + \ldots$
$^1\Phi_2 = -0.845(\pi_1^* \leftarrow n_{-2}) + \ldots$
$^1\Phi_3 = 0.888(\pi_1^* \leftarrow \pi_0) + \ldots$
$^1\Phi_4 = 0.823(\pi_1^* \leftarrow \pi_{-1}) + \ldots$

TABLE 11

Experimental[a] and calculated properties of 3-nitroanisole

Φ_i	*Symmetry*	*E* (eV)		*f*		μ (debyes)
		Calculated	*Experimental*	*Calculated*	*Experimental*	*Experimental*
0	A′	—	—	—	—	3.7
1	A″	2.92	3.35	10^{-4}		
2	A″	3.33		0		
3	A′	4.20	3.9 - 4.1	0.07	0.04	8.8
4	A′	4.88	4.7 - 4.9	0.188	0.12	
5	A′	5.26	5.5 - 5.7	0.087		
6	A′	5.84	5.85	0.299		

[a] Data from refs. 57 and 71.

TABLE 12

Localization of the molecular orbitals of 3-nitroanisole

	n_0	n_{-1}	n_{-2}	π_{-1}	π_0	π_1^*
P_{NO_2}	0.45	0.45	0.85	0.03	0.00	0.70

tions on the NO_2 group [65]. Since there is a great resemblance in electronic properties of an NH_2 and an OCH_3 group it may be anticipated that an *ab initio* calculation would also localize the first two excitations in 3-NA on the NO_2 group. The *ab initio* calculation on 3-nitroaniline yields an energy separation between $^1\Phi_1$ and $^1\Phi_2$ of 0.7 eV, whereas semiempirical methods with neglect of differential overlap predict values between 0.3 and 0.4 eV [59, 64, 66]. Since neglect of overlap between the two neighbouring lone pair atomic orbitals seems a serious defect in treating the splitting between the n_0 and n_{-1} MOs, we regard the *ab initio* value of 0.7 eV as more reliable than the CNDO results and expect that the energy gap between $^1\Phi_1$ and $^1\Phi_2$ in nitrobenzene and 3-NA and the corresponding two pairs of states in 3,5-DINA will also be around 0.7 eV.

The CNDO/S–CI calculation places $^1\Phi_1$ 0.4 eV lower in energy than estimated experimentally. In nitrobenzene, 3,5-DINA and other nitro aromatic compounds the corresponding $^1\Phi_1$ states are also calculated to be

too low [64]. We think therefore that the relative energies of the singlet excited states are estimated in a better way by adopting the ordering of the $\pi\pi^*$ levels from the CNDO/S–CI calculations and then positioning $^1\Phi_1$ according to the experimental value and taking an energy gap of 0.7 eV between $^1\Phi_1$ and $^1\Phi_2$. In this manner $^1\Phi_2$ is positioned above $^1\Phi_3$. Finally we note that the presence of the electron-donating OCH_3 group in 3-NA lowers the excitation energy of the charge transfer state $^1\Phi_3$ significantly compared with nitrobenzene, where it is labelled $^1\Phi_4$ (Fig. 23).

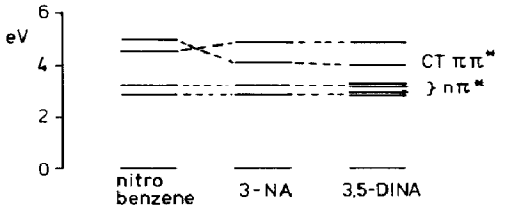

Fig. 23. Electronic energy level diagram obtained from CNDO/S–CI calculations: - - - -, connects related states.

4.1.2.3. 3,5-dinitroanisole. The results of the calculation for 3,5-DINA, together with some experimental data, are gathered in Tables 13 - 15. The calculated transition energies are nearly identical with those of 3-NA. The main difference from 3-NA is that we now obtain two pairs of nearly degenerate $n\pi^*$ states, ($^1\Phi_1$, $^1\Phi_2$) and ($^1\Phi_3$, $^1\Phi_4$). The n MOs are largely localized on the NO_2 groups as can be seen in Table 14. The π_1^* and π_2^* MOs may be regarded as symmetric and antisymmetric linear combinations of π_1^* of 3-NA and 5-NA. From the orbital populations and the wavefunction expansions we calculate that 70% of $(^1\Phi_1)^2$ arises from configurations in which the excitation is almost entirely localized on the NO_2 group(s), the remaining 30% is contributed by a configuration which involves MOs which are localized for about 50% on the NO_2 groups. Therefore excitation to $^1\Phi_1$ may be regarded as a local excitation of the NO_2 groups. The same applies for $^1\Phi_2$, $^1\Phi_3$ and $^1\Phi_4$. The near degeneracy of ($^1\Phi_1$, $^1\Phi_2$) and ($^1\Phi_3$, $^1\Phi_4$) reflects that the two NO_2 groups have very little interaction. Consequently the same reasoning as for 3-NA regarding the position of the energy levels of these $n\pi^*$ states and energy gap between $^1\Phi_{1,2}$ and $^1\Phi_{3,4}$ applies here, *i.e.* we take $E_{3,4}-E_{1,2} \approx 0.7$ eV and $E_{1,2}$ about 0.4 eV higher than calculated. The weak absorption band around 3.4 eV can now be assigned to a transition from $^1\Phi_0$ to $^1\Phi_1$ or $^1\Phi_2$ or to both.

State $^1\Phi_5$ is a charge transfer state similar to those encountered in nitrobenzene ($^1\Phi_4$) and in 3-NA ($^1\Phi_3$). The absorption band at 4.13 eV is thought to arise from a transition from $^1\Phi_0$ to $^1\Phi_5$. In this state electronic charge is transferred from the anisole part of the molecule to both NO_2 groups. This is reflected in the increase in dipole moment compared with the ground state. The energy gap ΔE between $^1\Phi_{1,2}$ and $^1\Phi_5$ is estimated from the gas phase spectrum to be 0.7 eV. In solvents this gap will be reduced to $\Delta E < 0.4$ be-

TABLE 13

Truncated wavefunctions of 3,5-dinitroanisole

	E (eV)
$^1\Phi_1 = -0.625(\pi_2^* \leftarrow n_0) - 0.553(\pi_1^* \leftarrow n_{-1}) + \ldots$	
$^1\Phi_2 = -0.585(\pi_1^* \leftarrow n_0) - 0.579(\pi_2^* \leftarrow n_{-1}) + \ldots$	
$^1\Phi_3 = 0.458(\pi_2^* \leftarrow n_{-3}) + 0.458(\pi_1^* \leftarrow n_{-4}) + \ldots$	
$^1\Phi_4 = -0.466(\pi_2^* \leftarrow n_{-3}) - 0.476(\pi_1^* \leftarrow n_{-3}) + \ldots$	
$^1\Phi_5 = 0.885(\pi_1^* \leftarrow \pi_0) + \ldots$	
$^1\Phi_6 = -0.945(\pi_2^* \leftarrow \pi_0) + \ldots$	
$^3\Phi_1 = -0.589(\pi_1^* \leftarrow \pi_{-2}) - 0.698(\pi_2^* \leftarrow \pi_{-2}) + \ldots$	1.44
$^3\Phi_2 = -0.649(\pi_1^* \leftarrow \pi_{-3}) + 0.647(\pi_2^* \leftarrow \pi_{-3}) + \ldots$	1.45
$^3\Phi_3 = -0.635(\pi_4^* \leftarrow \pi_0) + \ldots$	2.91
$^3\Phi_4 = -0.625(\pi_2^* \leftarrow n_0) - 0.553(\pi_1^* \leftarrow n_{-1}) + \ldots \approx {}^1\Phi_1$	2.96
$^3\Phi_5 = -0.585(\pi_1^* \leftarrow n_0) - 0.579(\pi_2^* \leftarrow n_{-1}) + \ldots \approx {}^1\Phi_2$	2.96
$^3\Phi_6 = 0.868(\pi_1^* \leftarrow \pi_0)$	3.02

TABLE 14

Localization of the molecular orbitals of 3,5-dinitroanisole

	n_0	n_{-1}	n_{-2}	n_{-3}	n_{-4}	π_2^*	π_1^*	π_0	π_{-1}	π_{-2}	π_{-3}
$P_{(NO_2)_3}$	0.23	0.41	0.92	0.45	0.0	0.35	0.4	0.006	0.04	0.0	1.0
$P_{(NO_2)_5}$	0.23	0.41	0.0	0.45	0.92	0.35	0.4	0.006	0.04	1.0	0.0

TABLE 15

Experimental and calculated properties of 3,5-dinitroanisole

$^1\Phi_i$	*Symmetry*	E (eV)		f		μ (debyes)	
		Calculated	*Experimental*	*Calculated*	*Observed*	*Calculated*	*Experimental* [12]
0	A′	—	—	—	—	7.48	4.0
1	A″	2.96	≈3.4	10^{-5}	50	4.03	
2	A″	2.96		10^{-4}		5.68	
3	A″	3.35		10^{-4}		4.15	
4	A″	3.36		10^{-6}		8.37	
5	A′	4.17	4.13	0.097	3000	11.27	8.5
6	A′	4.80	4.8	10^{-4}		16.44	
7	A′	5.17	5.2	0.353		14.16	

cause the $n\pi^*$ and $\pi\pi^*$ states shift in opposite directions. In cases where hydrogen bonding occurs $^1\Phi_{1,2}$ and $^1\Phi_5$ might even reverse in order.

With respect to the triplet manifold the CNDO/S–CI method predicts two nearly degenerate $\pi\pi^*$ states as the first two triplet states. These two states are highly localized on the NO_2 groups and similar to the first triplet

state in nitrobenzene. As before, we think that the singlet–triplet splitting is overestimated in the calculation owing to the full localization of the MOs on the oxygen atoms of the NO_2 groups and therefore these two triplet states will actually lie much higher. This leaves for the first four triplet states the degenerate pair of $n\pi^*$ states $^3\Phi_4$ and $^3\Phi_5$, the charge transfer state $^3\Phi_6$ and the state $^3\Phi_3$, which represents a local excitation of the anisole moiety. As pointed out earlier the ordering of the triplet states cannot be established by the CNDO/S–CI calculation. We assume that the $^3n\pi^*$ states ($^3\Phi_{4,5}$) will be the first two triplet states slightly below $^3\Phi_6$ (the charge transfer state) in non-hydrogen-bonding solvents.

At present there is no evidence for the existence of the $^3\Phi_{1,2}$ states. It may be anticipated that it will be difficult to discriminate between a localized $^3n\pi^*$ excitation and a localized $^3\pi\pi^*$ excitation, because both excitations may render the NO_2 group very reactive [66]. Indeed a localized $^3\pi\pi^*$ excitation may also lead to a deformation of the excited state potential energy surface and thereby to high non-radiative decay rates [66].

In conclusion we may say that the CNDO/S–CI method predicts transition energies, oscillator strengths, polarization directions and dipole moments in fair agreement with the experiments as far as singlet states are concerned, thereby providing us with a reasonable insight into the types of excited states that are involved and how for a group of molecules these states are related. For the nitroanisoles we conclude that there is a low-lying $n\pi^*$ singlet state (two states in 3,5-DINA) which is highly localized on the NO_2 group, with a charge transfer $\pi\pi^*$ state in its vicinity. The same probably applies for the triplet states. The energy level of the $n\pi^*$ states hardly shifts in going from nitrobenzene to 3-NA or 3,5-DINA, whereas the position of the charge transfer state is rather sensitive to the type of aromatic ring to which it is attached, as is shown in Fig. 23. Starting from Fig. 23 we derived the energy level scheme given in Fig. 1 and used in our discussion of the relaxation of 3,5-DINA.

4.1.3. Photoelectron spectra

Experimental information on the electronic structure of the nitroanisoles can be obtained from photoelectron spectra. The observed photoelectron spectroscopy bands can be correlated with specific SCF MOs from the CNDO/S–CI calculations. For nitroanisoles and nitrophenol such correlations have been made with CNDO/2 calculations [75].

The photoelectron spectrum of 3,5-DINA, shown in Fig. 24, has been measured by using the He(I) 21.21 eV resonance line for excitation. The resulting vertical ionization potentials together with those of 3-NA and of nitrobenzene are given in Tables 16 and 17.

The shape of the spectrum of 3,5-DINA is very similar to that of 3-NA [75]. Only small shifts in the positions of some of the bands are observed. The first two bands of 3,5-DINA (and 3-NA) and nitrobenzene can be assigned to ionizations from π MOs localized on the anisole and benzene part of the molecules [75]. The two bands appear at ionization energies of about

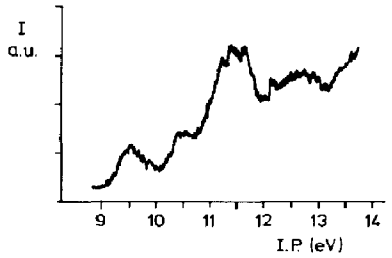

Fig. 24. Photoelectron spectrum of 3,5-DINA.

TABLE 16

Photoelectron spectroscopy band	*Vertical ionization potentials* (eV) *for the following molecules*		
	Nitrobenzene[a]	*3-NA*[a]	*3,5-DINA*
1	9.93	9.01	9.4
2	10.32	9.87	10.22
3	11.01	10.86	11.2
4	11.23	11.14	11.35

[a] Data from ref. 21.

TABLE 17

MO	*SCF MO energies* (eV) *for the following molecules*		
	Nitrobenzene	*3-NA*	*3,5-DINA*
π_0	−10.58	−9.99	−10.56
π_{-1}	−10.78	−10.74	−11.49
n_0	−11.85	−12.59	−13.14
$\pi_{-2}(NO_2)$	−12.67	−11.86	−12.09

0.7 eV and about 1.1 eV higher for 3-NA and 3,5-DINA respectively than the corresponding bands in anisole. This increase in ionization potential can be explained by the electron-withdrawing effect of the NO_2 group(s) which stabilizes the π MOs. The stabilization is confirmed by the CNDO/S–CI calculation which predicts a stabilization of approximately 0.6 eV in going from 3-NA to 3,5-DINA. The third band can be identified with an ionization from the n orbitals localized on the NO_2 groups from the fact that the shape and position are similar to those of the same band in nitrobenzene. The same applies for the fourth band, which is assigned to the π_{NO_2} orbital. Both these MOs are localized on the NO_2 group and are not very sensitive to the type of aromatic system to which the NO_2 group is attached.

The above interpretation is supported by the CNDO/S–CI calculation. We observe in Tables 16 and 17 that the ordering of the MOs corresponds to

the one given above, with the exception of the two close lying MOs 3 and 4. The calculated ionization potentials are somewhat higher than the experimentally observed values; this may be understood because electron reorganization is not taken into account in the SCF orbital energies. The calculated values deviate by about 1 eV for the π MO ionization energies and by about 1.5 eV for the n MO ionization energies.

In conclusion, the photoelectron spectra support the CNDO/S–CI results and make them more convincing.

4.2. Hydrogen bonding of nitroanisoles

4.2.1. Ground state complexes

An important question in the discussion of the relaxation of excited 3,5-DINA molecules in hydrogen bonding solvents is whether or not 3,5-DINA forms hydrogen bonds in its electronic ground state. As 3,5-DINA has "non-bonding" electron pairs at both the OCH_3 and the NO_2 groups it might be expected to form one or more hydrogen bonds with solvent molecules. We have used IR spectroscopy to study the interaction of TFE and 3,5-DINA in dilute solutions. TFE was chosen because it is capable of forming strong hydrogen bonds and has itself a low degree of association [76, 77].

We focus our attention on the shift in frequency of the fundamental O—H stretching vibration due to hydrogen bonding. Figure 25, spectrum a, shows the absorption spectrum of a dilute solution of TFE (1.58×10^{-2} M) in CCl_4. The highest peak at 3625 cm^{-1} arises from the monomer alcohol and the weak and broad band around 3400 cm^{-1} is due to hydrogen-bonded clusters of TFE molecules [76, 77]. Figure 25, spectrum c, shows a new band at 3488 cm^{-1} which develops when anisole is added to the solution (anisole concentration, 0.1 M). At the same time the monomer peak decreases in intensity.

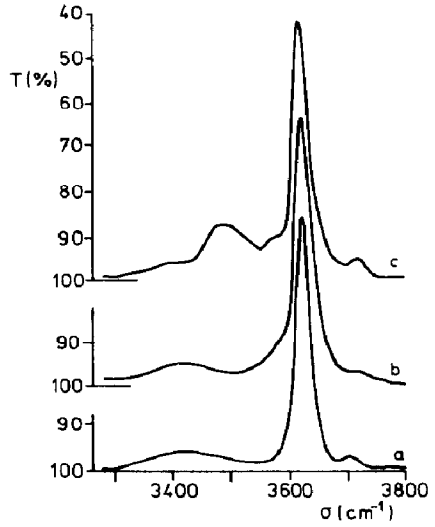

Fig. 25. IR absorption spectra: spectrum a, TFE in CCl_4; spectrum b, TFE + 3,5-DINA in CCl_4; spectrum c, TFE + anisole in CCl_4.

Another weak absorption band around 3580 cm^{-1} is also a consequence of the interaction between anisole and TFE. The band at 3488 cm^{-1} arises from a complex between the OH group of TFE and the OCH_3 group of anisole and the band at 3580 cm^{-1} is attributed to a complex of TFE and anisole, bonded via an interaction with the π electron system of the anisole [78].

The shift $\Delta\sigma$ in wavenumber of the O—H stretching vibration induced by the hydrogen bond is proportional to ΔH, the change in enthalpy due to formation of the complex. Using the relation between ΔH and $\Delta\sigma$ for TFE [77 - 79] we obtain a bonding enthalpy ΔH for anisole with TFE of −17.6 kJ mol^{-1} for the σ complex and a bonding enthalpy of ΔH_π of −3.3 kJ mol^{-1} for the π complex.

In Fig. 25, spectrum b, the spectrum of a solution of 3,5-DINA (0.1 M) and TFE in CCl_4 is presented. The concentration of the aromatic compound and the alcohols are each the same as in the previous cases. The absorptions due to the monomer alcohol and the clusters of alcohol molecules are again observed at 3625 cm^{-1} and around 3400 cm^{-1}. However, in contrast with the spectrum of TFE with anisole there is no well-resolved band which can be associated with complex formation between the alcohol and 3,5-DINA. Only a slight broadening at the bottom of the 3625 cm^{-1} band indicates the formation of very weak complexes with $\Delta H = -3.3$ kJ mol^{-1} [78]. Whether these complexes involve hydrogen bonds to the OCH_3 group, to the NO_2 group or to the benzene ring is difficult to say. A reduction in ΔH of the OCH_3 hydrogen bond and of the π complex is to be expected because of the introduction of the electron-withdrawing NO_2 groups. A good correlation between the electronegativity of the acceptor substituents and the shift in frequency has been found [78]. With the aid of this relationship we estimate $\Delta\nu$ of the OCH_3 hydrogen bond to be about 50 cm^{-1}, and $\Delta\nu \approx 0$ cm^{-1} for the π complex. Apparently only very weak hydrogen bonds to the OCH_3 group are involved. With respect to possible weak hydrogen bonds to the NO_2 groups it may be said that they cannot be excluded rigorously, although NO_2 groups are known to be extremely weakly basic [79, 80].

The question whether or not 3,5-DINA is complexed to a large extent when it is dissolved in concentrations of 10^{-3} mol l^{-1} or less in pure TFE, CH_3OH or H_2O cannot be answered definitively. The major difficulty arises from the unknown entropy effects. In a non-rigorous fashion it may be argued that the enthalpy of dimerization of TFE (−22.3 kJ mol^{-1}) is considerably larger than that for the complexation of TFE with 3,5-DINA. Therefore, if entropy effects for the two complexes do not differ too much, we expect no substantial complexation between 3,5-DINA and TFE. Since CH_3OH is less acidic than TFE the binding energy of the complex between CH_3OH and 3,5-DINA will be even smaller than that of the 3,5-DINA–TFE complex. From data on complexes of fluorinated and ordinary alcohols with the same acceptor molecules we estimate $\Delta H > -2.5$ kJ mol^{-1}. In contrast, CH_3OH has a much higher degree of self-association. At room temperature only 2% of the molecules are in the monomer form [81]. The above means

that 3,5-DINA in CH_3OH will show an even lower tendency to be hydrogen bonded than it does in TFE.

Finally, in pure H_2O the monomer concentration is estimated to be about 10^{-3} mol l^{-1} [59, 82]. The binding energy for the H_2O dimer is 19 kJ mol^{-1}, whereas the binding energy of the 3,5-DINA–H_2O complex is estimated to be smaller than 3.3 kJ mol^{-1}. Therefore again it seems improbable that 3,5-DINA is hydrogen bonded in aqueous solutions. The conclusion that 3,5-DINA is not hydrogen bonded when dissolved in H_2O or alcohols is supported by our earlier study on the triplet lifetime in CH_3OH. Here the triplet lifetime increases on lowering the temperature until a glassy state of the alcohol is reached, then the triplet lifetime becomes again very short [11, 39]. We concluded that the short-lived triplet state is not hydrogen bonded, whereas the long-lived triplet state appears after hydrogen bonding of the excited 3,5-DINA molecule. The latter step becomes impossible in a glassy solution. The very low solubility of 3,5-DINA in H_2O is also in accordance with the absence of hydrogen bonding between 3,5-DINA and H_2O.

In conclusion, we presented evidence that 3,5-DINA hardly forms any hydrogen bonds with TFE and probably none with CH_3OH and H_2O. In the following sections we shall assume that 3,5-DINA in its electronic ground state is non-hydrogen-bonded at the NO_2 groups in these solvents.

4.2.2. Excited state complexes

The hydrogen bonding interaction between the excited 3,5-DINA molecule and solvent molecules must be studied in an indirect manner. We have chosen the 3,5-DINA anion as a model compound for 3,5-DINA in its excited charge transfer states $^1\Phi_5$ and $^3\Phi_6$, because in both cases an unpaired electron occupies the π_1^* MO [83]. First we shall discuss the results of the ESR study of the anion in aqueous solutions and then the relation of the anion to the excited molecule.

4.2.2.1. 3,5-dinitroanisole anion in aqueous solutions. The spectrum of the radical anion of 3,5-DINA in a solution in CH_3CN has been given earlier [84], and is displayed in Fig. 26. From the pattern of lines it may be concluded that in this solution the two nitrogen nuclei are equivalent, *i.e.* the anion has approximately C_{2v} symmetry. The hyperfine coupling constant for each of the nitrogen atoms amounts to 4.41 G and that for the hydrogens to 2.63 G [84].

If H_2O is used as a solvent for the anion of 3,5-DINA the ESR spectrum becomes quite different. The spectrum, obtained at 300 K, is presented in Fig. 27. In addition to the lines assigned to the anion, indicated by arrows, the spectrum shows some weak lines due to reaction products of 3,5-DINA. The pattern of lines and the intensity distribution indicate a strong hyperfine interaction with a single nitrogen nucleus and three equivalent hydrogens. Such a coupling scheme leads to a sequence of three groups of four lines each, exactly as found in the spectra. Apparently the spin density of the unpaired electron here is localized on only one of the NO_2 groups on the characteristic time scale of the ESR experiment.

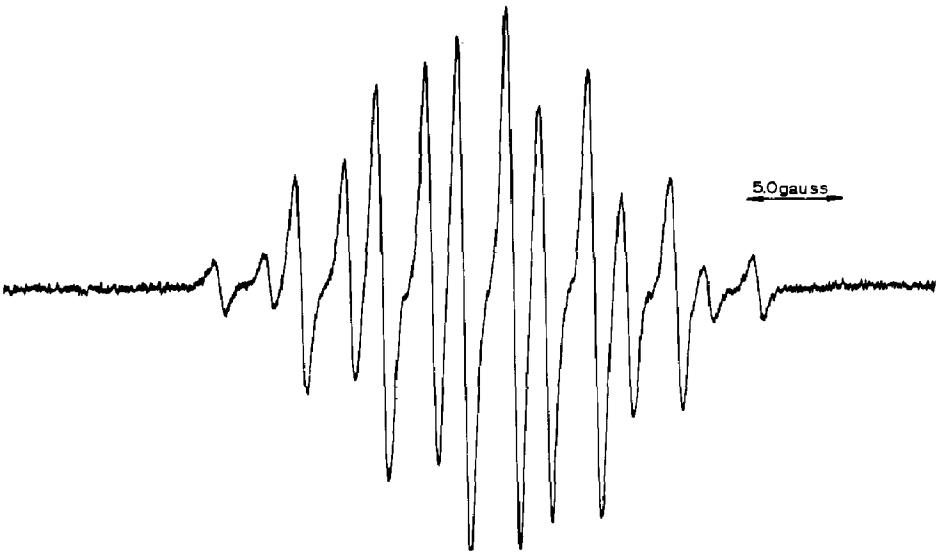

Fig. 26. ESR spectrum of the anion of 3,5-DINA in CH_3CN (T = 300 K).

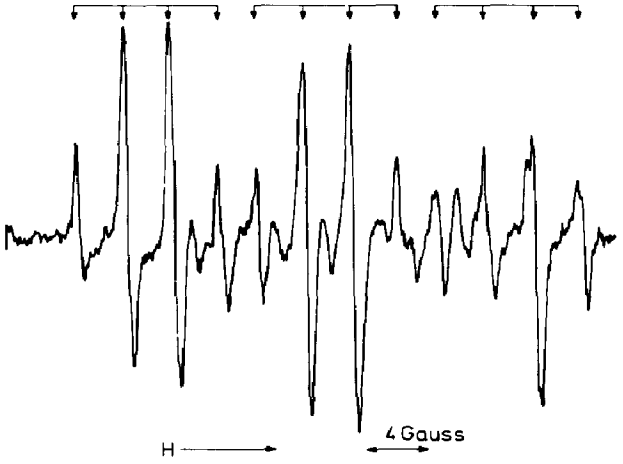

Fig. 27. ESR spectrum of the anion of 3,5-DINA in aqueous solution.

The low field line of the spectrum has been chosen for a detailed study of its width and structure as a function of temperature. Figure 28, spectrum a, shows this line at room temperature (300 K) and Fig. 28, spectrum b, at 273 K. A lowering of the temperature yields two new lines up field. The splitting between these neighbouring lines is 0.15 G. Next to every component in the spectrum of Fig. 27 two such additional lines appear on lowering the temperature. We attribute the tripling of the number of lines in the spectrum to the hyperfine interaction with the nitrogen nucleus of the second NO_2 group of the anion.

To explain the transition from a system with a single line to a system with two nitrogen hyperfine couplings the model illustrated in Fig. 29 is used. Here each NO_2 group is considered to have its own H_2O molecule available for hydrogen bonding. But at any instant only *one* of the two NO_2

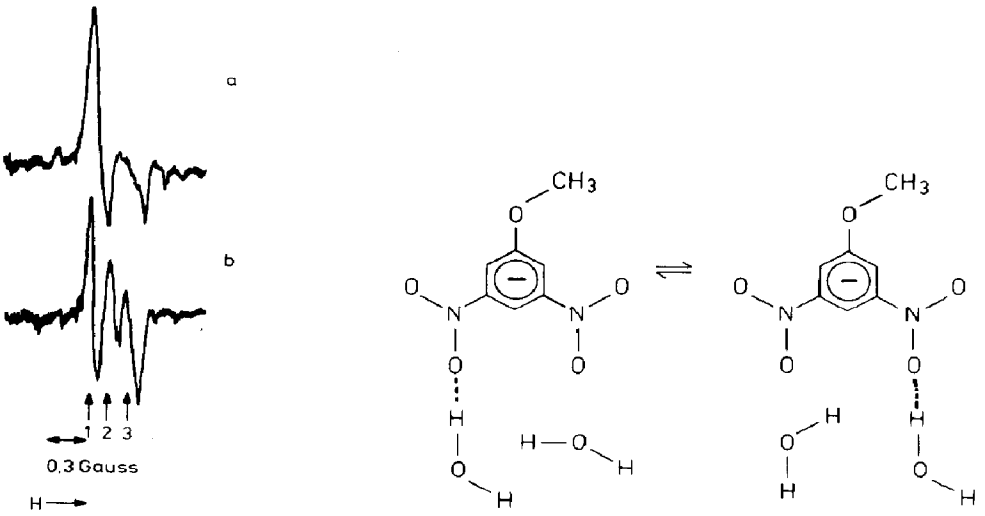

Fig. 28. Low field lines of the ESR spectrum of the 3,5-DINA anion in H_2O: at 300 K (spectrum a) and 273 K (spectrum b). The anion of 3,5-DINA was generated *in situ* by mixing a saturated solution of 3,5-DINA in H_2O with a 0.1 M solution of sodium dithionite in H_2O in a flow cell (mixing ratio, 12:1).

Fig. 29. Site exchange model for the hydrogen bonding of the NO_2 groups of the anion of 3,5-DINA. The negative charge of the anion becomes localized on the hydrogen-bonded NO_2 group.

groups is hydrogen bonded, either at the 3 or the 5 position of the benzene ring. This implies a fluctuation of the hyperfine splitting of the two nitrogen atoms, since switching from one hydrogen bond to the other will modify the spin density distribution over the molecule.

The model in Fig. 29 is a specific example of the "site exchange" model, generally used for the explanation of alternating linewidths in magnetic resonance spectra [85, 86]. In our case we assume that by hydrogen bonding of a given NO_2 group the spin density on its nitrogen nucleus is increased and simultaneously decreased on the other nitrogen nucleus. The hyperfine splittings of the two nitrogen nuclei then vary in magnitude. They will be denoted by a_N and a_N'. The diagram of Fig. 30 gives a schematic explanation of the pattern of lines and linewidths to be expected. It is assumed that no nuclear spin transitions occur during the site exchange. The diagram starts with $a_N \gg a_N'$ and considers only the nitrogen splittings. Each of the nine lines shown will yield a group of four lines when the additional splitting of three equivalent hydrogen nuclei is taken into account.

The position of the lines with respect to the central line as origin is indicated in the diagram. It is seen that after interchange of a_N and a_N' lines 1, 5 and 9 keep their original position, but lines 2 and 4, 6 and 8, and 3 and 7 interchange their positions pairwise. When the exchange frequency is high compared with the difference in resonance frequency of the lines in a pair, that pair will coalesce into a single line at the mean frequency. There-

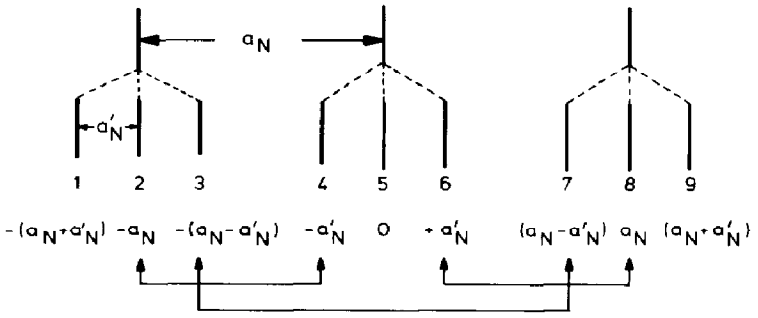

Fig. 30. Diagram for the nitrogen splitting in the ESR spectrum of the anion of 3,5-DINA.

fore fast exchange is expected to lead to a spectrum with five groups of lines, just as observed for the solution of the 3,5-DINA anion in CH_3CN. At intermediate exchange rates lines 2, 3, 4, 6, 7 and 8 will broaden and may become too diffuse to be observable. Nevertheless lines 1, 5 and 9 will remain sharp. Owing to the hydrogen splitting each of these lines breaks up into four lines. Apparently this is realized for the solution of the anion in H_2O, as was shown in Fig. 27.

At a sufficiently low temperature the exchange rate will be lowered to such an extent that the complete system of nine groups of four lines becomes observable. The spectrum shown in part in Fig. 28 reveals the reduction in the exchange rate. The small splitting of 0.15 G, due to the second nitrogen nucleus, can now be observed. In the upper part of Fig. 28, lines 2 and 3 are almost washed out owing to the increased rate of exchange.

The effects of site exchange on the widths and positions of the ESR lines may be treated quantitatively by using the modified Bloch equations, which allow for exchange between the two sites [85, 86]. In the limiting case of slow exchange the following expression then holds for the transverse relaxation time T_2:

$$\frac{1}{T_2'} = \frac{1}{T_2} + \frac{1}{\tau} \tag{43}$$

Here T_2 and T_2' apply respectively to the lines unaffected by exchange and to the exchange-broadened lines and τ is the mean time of residence on a site. An estimate of τ can be obtained by comparing the widths of the two types of lines. The determination of the width of the unaffected line offers no special problem; the width of the broadened line has to be estimated in an indirect manner with the aid of the following expression [87]:

$$\Delta H_b = \left(\frac{A_u}{A_b}\right)^{1/2} \Delta H_u \tag{44}$$

Here ΔH is the width and A the amplitude of a line; b and u refer to the broadened and unaffected lines. From eqns. (43) and (44)

$$\tau^{-1} = 2.6 \times 10^{7} \left\{ \left(\frac{A_u}{A_b} \right)^{1/2} - 1 \right\} \Delta H_u \qquad (45)$$

is obtained. For the anion of 3,5-DINA in H_2O a value $\tau = 1 \times 10^{-6}$ is obtained from eqn. (45) and from a comparison with reported spectra of the anion of 1,3-dinitrobenzene [87 - 89]. The ESR spectrum of the latter anion reveals also two equivalent nitrogen nuclei in non-hydrogen-bonding solvents and a site exchange of a hydrogen bond from one NO_2 group to the other in hydrogen bonding solvents. The lifetime of the hydrogen bond was found to vary from 1×10^{-6} s, for the 1,3-dinitrobenzene anion in H_2O, to 2×10^{-9} s, when it was in a 80:20 (by volume) mixture of DMF:CH_3CH_2OH. These lifetimes are nearly equal to those of the 3,5-DINA anion in the same solvent.

4.2.2.2. Relation between anion and excited molecule. To explain the asymmetrical charge distribution observed in the anions of 3,5-DINA and other dinitrobenzenes and to understand the similarity between the behaviour of the anion and the excited molecule we consider their electronic structure. The asymmetrical charge distribution over the NO_2 groups can be described with an MO, which is a linear combination of two π^* MOs each describing a symmetrical charge distribution. The latter two MOs are indicated as π_1^* and π_2^* and have high electron densities on the NO_2 groups. The MO $\pi_{1,a}^*$ given by

$$\pi_{1,a}^* = \frac{1}{2^{1/2}} (\pi_1^* - \pi_2^*) \qquad (46)$$

has a high electron density on one NO_2 group and a low density on the other NO_2 group. The asymmetrical situation might be realized if the net energy gained by hydrogen bond formation is larger than the energy needed to form the asymmetrical charge distribution, *i.e.* if $|E_{HB,a} - E_{HB,s}| > (E\pi_2^* - E\pi_1^*)/2$. Here $E_{HB,a}$ and $E_{HB,s}$ are the hydrogen bonding energies of the molecules with an asymmetrical and a symmetrical charge distribution respectively. In other words the ease with which an asymmetrical charge distribution can be formed will depend on the magnitude of the gap between the energies of π_1^* and π_2^* for a particular nitro compound. It has indeed been observed for a number of dinitro aromatic anions that the magnitude of this energy gap determines whether asymmetrical structures can arise or not [88].

The relation between the anion and the excited charge transfer state may be envisaged as follows. In a zero-order approximation we can say that in both the anion and the excited state the π_1^* MO is occupied by a single electron [83]. The difference between the two is the electron hole in orbital π_0 in the excited molecule. The orbital π_0 is mainly localized on the anisole part of the molecule and orbital π_1^* is localized on the NO_2 groups. As far as the charge distribution over the NO_2 groups is concerned we may expect that the anion is a good model of the excited molecule. We thus expect that in the excited molecule also hydrogen bonds will be formed between solvent

TABLE 18

Electron density differences between the ground state and excited states (NO_2 groups only) for 3,5-dinitroanisole and 3,5-dinitroanisole–H_2O

Atom	*Electron density differences for the following states* Φ_i					
	1	2	3	4	5	6
3,5-DINA						
N(1)	0.08	0.08	0.13	0.13	0.12	0.16
N(2)	0.08	0.08	0.12	0.13	0.11	0.17
O(1)	−0.08	−0.07	−0.10	−0.03	0.07	0.09
O(2)	−0.09	−0.11	−0.10	−0.03	0.07	0.09
O(3)	−0.12	−0.09	−0.06	−0.14	0.06	0.10
O(4)	−0.06	−0.09	−0.08	−0.16	0.06	0.10
3,5-DINA + H_2O						
N(1)	0.04	0.13	0.09	0.17	0.19	0.12
N(2)	0.12	0.04	0.19	0.07	0.05	0.19
O(1)	−0.05	−0.01	0.03	−0.19	0.12	0.06
O(2)	−0.06	−0.09	0.02	−0.26	0.11	0.06
O(3)	−0.10	−0.10	−0.22	0.02	0.03	0.12
O(4)	−0.12	−0.06	−0.27	0.01	0.03	0.12

Atoms O(1) and O(2) are bound to atom N(1); atoms O(3) and O(4) are bound to atom N(2).

molecules and the NO_2 groups, which will influence the charge distribution in the same manner as in the anion.

No direct experimental evidence can be given for the occurrence of such an asymmetrical charge distribution in the excited charge transfer state, which is stabilized by hydrogen bonding. However, a CNDO/S–CI calculation on the supermolecule 3,5-DINA–H_2O reveals indeed an asymmetry in the charge distribution just as expected from the simple arguments given. A length of 1.6 Å has been used for the hydrogen bond [90]. The electron density differences obtained from the calculation are given in Table 18. The atom numbering in Fig. 31 has been used. It appears that the $^1\Phi_5(\pi_0\pi_1^*)$ state becomes strongly polarized by the hydrogen bond. All the electronic charge (0.42 electron) which is transferred to both NO_2 groups in the excited state, when no hydrogen bond is present, is now transferred to the NO_2 group that is hydrogen bonded. The polarization effect on the excited state is also reflected in the wavefunction describing this state. The π^* MOs of interest are given in Table 19. Here π_1^* and $\pi_{1,a}^*$ are the virtual MOs used in the leading singly excited configurations of the wavefunctions for 3,5-DINA and 3,5-DINA–H_2O respectively. π_2^* is an MO just above π_1^* of 3,5-DINA. It can be seen in Table 19 that $\pi_{1,a}^*$ is indeed a linear combination of π_1^* and π_2^*, resembling $(\pi_1^* - \pi_2^*)/2^{1/2}$. The calculated energy gap between π_1^* and π_2^* amounts to 0.26 eV and therefore the net energy gain due to asymmetrical hydrogen bonding must be larger than 0.13 eV (= 2.9 kcal mol^{-1}), which is not unreasonably high in view of the bonding energies involved.

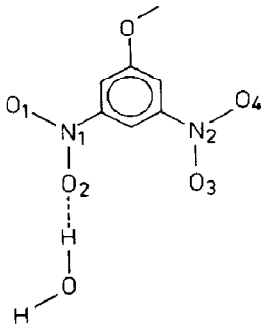

Fig. 31. Numbering of the atoms in Tables 18 and 19.

TABLE 19

Truncated wavefunctions and self-consistent field molecular orbitals of the charge transfer $\pi\pi^*$ state of 3,5-dinitroanisole and 3,5-dinitroanisole–H_2O (coefficients of the P_x atomic orbitals)

Atom	*P_x coefficients for the following orbitals*[a]			
	π_1^*	π_2^*	$\pi_{1,a}^*$	$(\pi_1^* - \pi_2^*)/2^{1/2}$
N(1)	+0.367	−0.397	+0.483	+0.54
N(2)	−0.319	−0.428	−0.191	+0.07
O(1)	−0.300	+0.309	−0.391	−0.43
O(2)	−0.308	+0.309	−0.376	−0.43
O(3)	+0.269	+0.336	0.168	0.05
O(4)	+0.264	+0.338	0.162	0.05
E (eV)	−3.05	−2.79		

Atoms O(1) and O(2) are bound to atom N(1); atoms O(3) and O(4) are bound to atom N(2).

[a] $^1\Phi_5 = 0.885(\pi_1^* \leftarrow \pi_0) + \ldots$ 3,5-DINA; $^1\Phi_5 = 0.875(\pi_{1,a}^* \leftarrow \pi_0) + \ldots$ 3,5-DINA + H_2O.

Other indirect evidence for asymmetrical hydrogen bonding of excited 3,5-DINA follows from the comparison made in Table 20. There the lifetime of the hydrogen bond deduced from the ESR linewidth measurements of the 3,5-DINA radical anion is compared with the lifetime of the triplet state of the 3,5-DINA molecule. Later we shall show that the lifetime of the triplet state in the hydrogen bonding solvents is primarily determined by the rate of dissociation of the hydrogen bond between the excited molecule and the solvent. The mixed solvent systems H_2O–DMF and H_2O–CH_3CN used in the two experiments are so chosen that they have comparable H_2O concentrations. The lifetimes of the ionic and molecular species prove to be nearly equal in pure H_2O and show the same sensitivity to addition of a non-hydrogen-bonding solvent. Therefore we conclude that the anion is very similar to the excited state with respect to the charge distribution, especially on the NO_2 groups. This means that hydrogen bonding of the excited 3,5-DINA molecule at an NO_2 group leads to a polarization of the charge

TABLE 20

Solvent	*Lifetime of the hydrogen bonds* (s)	
	3,5-DINA anion	*3,5-DINA triplet*
H_2O	$\approx 1 \times 10^{-6}$	3.5×10^{-6}
H_2O:DMF (20:80) [87]	2×10^{-9}	—
H_2O:CH_3CN ($\chi_{H_2O} = 0.2$)	—	2×10^{-9}

distribution and localization of the charge on the bonded NO_2 group. Because of the amount of charge involved (0.42 electron) we expect these hydrogen bonds to be rather strong [70, 90].

4.3. Decay of hydrogen-bonded triplet states of nitroanisoles

4.3.1. Kinetic scheme for the decay of the lowest triplet state

In the preceding sections we have established that 3,5-DINA when dissolved in a hydrogen bonding solvent is probably not hydrogen bonded and that hydrogen bonding takes place between 3,5-DINA in its $^1\pi\pi^*$ charge transfer state and the solvent. It is therefore logical to enquire whether dissociation of the hydrogen bonds plays an important role in the relaxation of the triplet state of 3,5-DINA.

The kinetic scheme for describing the decay of T_0 is given in Fig. 32(a). It involves the hydrogen-bonded and non-hydrogen-bonded triplet state of 3,5-DINA and its electronic ground state. The solution of the kinetic equations of this scheme is given at the end of this section. The scheme of Fig. 32(a) can be reduced to the simple two-step decay model of Fig. 32(b) for the following reasons. After excitation of 3,5-DINA dissolved in solvent systems with a high concentration of hydrogen bonding molecules, mainly hydrogen-bonded triplet states are formed via the route $S_i \rightarrow S_{i,\,HB} \rightarrow T_{0,\,HB}$. This leads to the initial conditions $C_{T_0}(t = 0)$ and $C_{T_{0,\,HB}}(t = 0) = C_0$. We have shown that the rate of decay of the non-hydrogen-bonded triplet state T_0, *i.e.* $^3n\pi^*$, in CH_3CN–H_2O mixtures is approximately equal to that of T_0 in CH_3CN. Therefore we may take $k_3 \approx 10^9\ s^{-1}$. In contrast, we made it plausible that the rate of reaction between the $^3n\pi^*$ state T_0 and a hydrogen bonding molecule is very low, *i.e.* $k_1 \ll k_3$. The lifetime of the transient absorption $T_n \leftarrow T_{0,\,HB}$ is generally longer than 50 ns for 3,5-DINA in hydrogen bonding solvents. This means that k_2 and k_4 are less than or equal

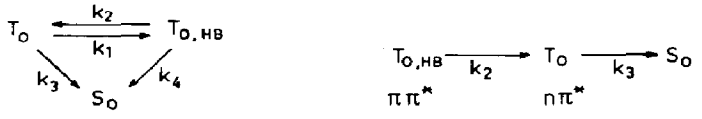

(a) (b)

Fig. 32. (a) Complete kinetic scheme describing the formation and decay of the hydrogen-bonded triplet state of 3,5-DINA; (b) simplified scheme for the decay of the hydrogen-bonded triplet state of 3,5-DINA.

to 2×10^7 s^{-1} and that k_3 is very much greater than k_2 and k_4. Later it will appear that $k_2 \gg k_4$ applies in the present situation. If the above conditions are valid then the decay of $T_{0,HB}$ is described by the two-step process, in which the dissociation reaction is the rate-limiting step. The lifetime of $T_{0,HB}$ is then given by $\tau = k_2^{-1}$, and the temperature dependence is determined by the temperature dependence of k_2.

4.3.2. The triplet state of 3,5-dinitroanisole in alcohols and H_2O

The temperature dependence of the triplet lifetime τ_T has been determined in the solvents HFP-2, TFE, CH_3OH and H_2O. All oxygen was removed from the solvents by repeated degassing or by flushing with argon. In all cases a monoexponential decay is observed. The Arrhenius plots $k_T = A \exp(-E_a/RT)$ are shown in Figs. 33 and 34. The parameters A and E_a are given in Table 21 together with the activation entropy calculated according to eqn. (58). Table 21 shows that the activation energy increases in the order CH_3OH < TFE < HFP-2. This is exactly the order in which the strength of a hydrogen bond between these alcohol molecules and any hydrogen bond acceptor increases [76, 77]. The rather high values of E_a indicate a strong hydrogen bond, which is expected for a hydrogen bond to a negatively charged NO_2 group [9]. The trend in E_a strongly supports the idea that dissociation of the hydrogen bonds is indeed the rate-limiting step in the decay

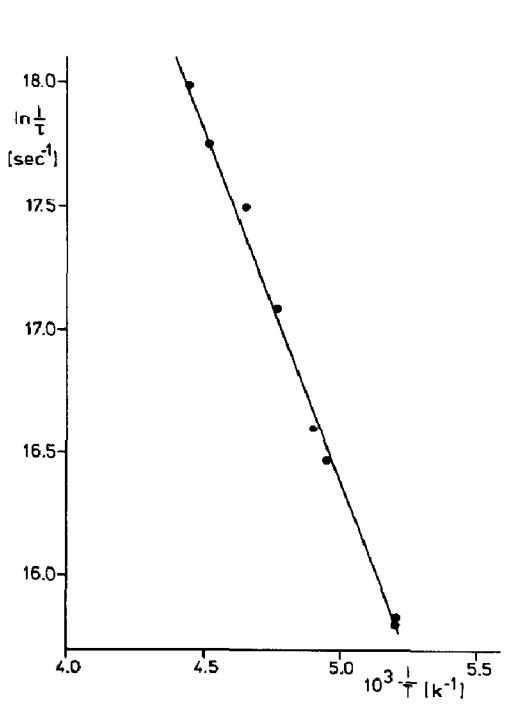

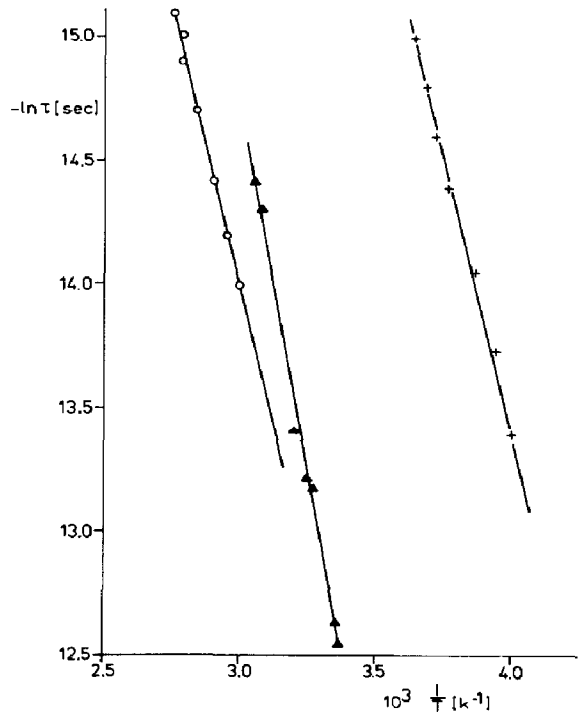

Fig. 33. Arrhenius behaviour of the inverse of the triplet lifetime of 3,5-DINA in CH_3OH.

Fig. 34. Arrhenius behaviour of the inverse of the triplet lifetime of 3,5-DINA in H_2O (○), HFP-2 (▲) and TFE (+).

TABLE 21

Arrhenius parameters for the inverse of the triplet lifetime of 3,5-dinitroanisole

Solvent	A (s^{-1})	E_a (kJ mol^{-1})	$(\Delta S^\circ)^\ddagger$ (J mol^{-1} K^{-1})
HFP-2	4.3×10^{13}	50.4	+7.8
TFE	2.9×10^{13}	36.1	+4.5
CH_3OH	1.2×10^{13}	22.7	−2.8
H_2O	4.8×10^{11}	36.1	−29.7

process of the triplet state. In going from HFP-2 to H_2O the activation entropy decreases considerably as can be seen in Table 21. An explanation of this phenomenon may be found by taking the self-association of the solvents into account. It is known that liquid H_2O shows a considerable structure owing to its strong self-association [91]. H_2O molecules can participate in three hydrogen bonds simultaneously and so three-dimensional structures may be formed in the liquid. This structure is very sensitive to addition of other solvents, which may destroy or enhance the structure. For instance, small amounts of *tert*-butanol promote solvent structure whereas 1,4-dioxane destroys it [91, 92]. If an excited molecule forms hydrogen bonds with H_2O molecules, these H_2O molecules can no longer participate in an ordered structure, which may exist near the solute or even around a hydrophobic part of it [87]. Therefore it is quite conceivable that the process of dissociation of hydrogen bonds between solute and solvent molecules would be accompanied by the simultaneous formation of a more structured region near or around the solute. Under such circumstances the dissociation process may well have a negative entropy of activation. In alcohols a similar effect may be present although the degree of self-association here is less pronounced because an alcohol molecule can only participate in two hydrogen bonds simultaneously. In the series CH_3OH, TFE and HFP-2 it has been established by IR studies that the self-association diminishes in going from CH_3OH to HFP-2 [76]. This is the same order in which $(\Delta S^\circ)^\ddagger$ decreases. The magnitude of the pre-exponential factor for the less self-associating solvents is close to the theoretical value $k_B T/h = 1.7 \times 10^{13}$ s^{-1}. Pre-exponential factors of this magnitude have often been observed for dissociation reactions in solution at room temperature [92].

4.3.3. The triplet state of 3,5-dinitroanisole in 1,4-dioxane–H_2O mixtures

We studied the temperature dependence of the triplet lifetime in solvent mixtures of 1,4-dioxane and H_2O to obtain more insight into the changes in the entropy of activation and the activation energy induced by alternation of the solvent composition. Mixtures of 1,4-dioxane and H_2O with a mole fraction around 0.9 were chosen because it is known that the association behaviour of the H_2O molecules changes dramatically in the

TABLE 22

Arrhenius parameters for the inverse of the triplet lifetime of 3,5-dinitroanisole in 1,4-dioxane–H_2O mixtures and the triplet lifetime at 20 °C

χ_{H_2O}	ln A	E_a (kJ mol^{-1})	$(\Delta S°)^{\ddagger}$ (J mol^{-1} K^{-1})	$\tau_{triplet}^{20\,°C}$ (ns)
0.85	25.58 ± 0.51	22.8 ± 1.4	−40.5 ± 4.3	70
0.90	25.34 ± 0.26	24.8 ± 0.7	−42.5 ± 2.2	215
0.95	25.21 ± 0.31	27.7 ± 0.8	−43.6 ± 2.6	800

vicinity of this value [92]. This change in association behaviour is also obvious from the change in triplet lifetime of 3,5-DINA illustrated in Table 22. The values of A, E_a and $(\Delta S°)^{\ddagger}$ were derived from the Arrhenius plots shown in Fig. 35. From Table 22 we may conclude that addition of 1,4-dioxane to H_2O leads to a slight increase in $(\Delta S°)^{\ddagger}$ and simultaneously to a decrease in E_a. Both effects shorten the triplet lifetime with increasing 1,4-dioxane content of the solvent.

It is interesting to compare the behaviour of the triplet lifetime of 3,5-DINA with the behaviour of the fluorescence quantum yield of acridine in the 1,4-dioxane–H_2O solvent mixtures. It has been shown that the dissociation process of the hydrogen bond between a solvent molecule and the excited acridine molecule may quench the fluorescence of acridine [93]. If we compare the activation energy and entropy of the two processes we observe a decrease in activation energy with about the same percentage for both molecules when the mole fraction of 1,4-dioxane is increased. Also the pre-exponential factor increases in both cases. In acridine there is only one site available for hydrogen bonding, namely the nitrogen lone pair. Therefore the observed decrease in E_a with increasing 1,4-dioxane concentration cannot result from a reduction in the number of hydrogen bonds. Probably it results from a smaller interaction between the H_2O molecule bonded to the

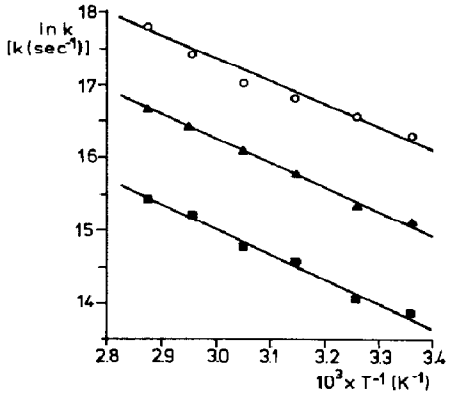

Fig. 35. Arrhenius behaviour of the inverse of the triplet lifetime of 3,5-DINA in 1,4-dioxane–H_2O mixtures: ■, $\chi_{H_2O} = 0.95$; ▲, $\chi_{H_2O} = 0.90$; ○, $\chi_{H_2O} = 0.85$.

acridine molecule and the other H_2O molecules. The same may be the case for 3,5-DINA where we expect that also only one strong hydrogen bond is formed between one NO_2 group and an H_2O molecule.

4.3.4. The triplet state of 3,5-dinitroanisole in CH_3CN–H_2O mixtures

The triplet lifetime of 3,5-DINA in CH_3CN–H_2O mixtures varies in the range 10 ns $< \tau <$ 3.5 μs when the solvent composition [11] varies in the mole fraction range $0.6 \leqslant \chi_{H_2O} \leqslant 1.0$. With the aid of picosecond kinetic measurements we have now been able to determine the triplet lifetime in solvent systems with $\chi_{H_2O} < 0.6$. For the actual experiment we took a mixture in which the mole fraction of H_2O is 0.2, because analyses of the triplet population kinetics indicate that in such a system already a large part of the triplet states is hydrogen bonded. Figure 36 shows the exponential decay curve obtained for 3,5-DINA in CH_3CN–H_2O with $\chi_{H_2O} = 0.2$. The triplet lifetimes derived from these decay curves are 789 ps and 1.8 ns, which are again lifetime enhancements due to hydrogen bonding. Figure 37 now displays the triplet lifetime as a function of the solvent composition over the full range. The triplet lifetime is seen to depend in a complicated way on χ_{H_2O}. In the range $0 < \chi_{H_2O} < 0.5$ we observe a change in $\tau_{triplet}$ by approximately a factor of 10, whereas in the range of $0.5 < \chi_{H_2O} < 1.0$ it changes

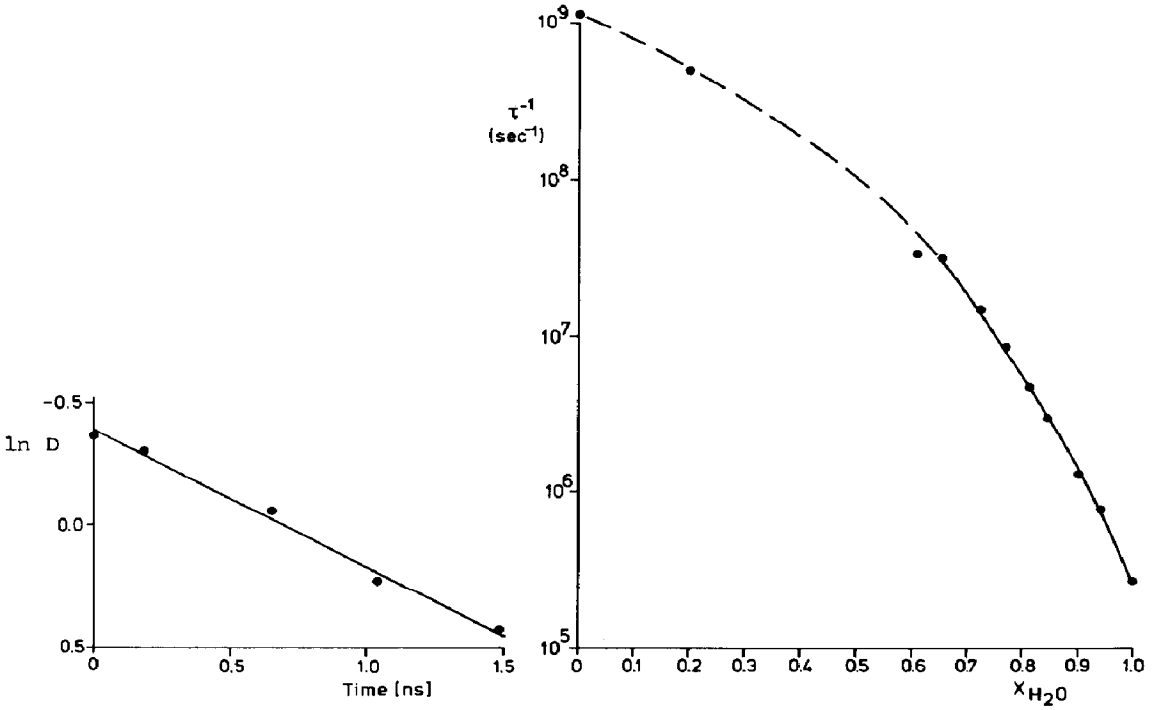

Fig. 36. Decay of the triplet–triplet absorption of 3,5-DINA in a CH_3CN–H_2O mixture with $\chi_{H_2O} = 0.2$ measured with the picosecond spectrometer ($\lambda_m = 430$ nm; $\lambda_{ex} = 353$ nm; $\tau = 1.8 \pm 0.1$ ns).

Fig. 37. Variation in the triplet lifetime of 3,5-DINA in CH_3CN–H_2O mixtures.

by a factor of 1000. At this moment we have no data on the temperature dependence of τ in the CH_3CN-H_2O systems and we are not able to pinpoint the exact cause of the lifetime variations. However, the strong variation in τ in the range $0.5 < \chi_{H_2O} < 1.0$ is probably caused in the same manner as we have already seen in 1,4-dioxane–H_2O mixtures. We again expect both $(\Delta S^\circ)^\ddagger$ and E_a to change because 1,4-dioxane and CH_3CN have a similar influence on the solvent structure. For a large excess of CH_3CN, in the CH_3CN-H_2O mixture there will be little or no H_2O structure left and the pre-exponential factor will then come close to 1.7×10^{13} s^{-1}. With a value E of 25.2 kJ mol^{-1} this yields a lifetime of 1.8 ns, close to what we observe for the solution with $\chi_{H_2O} = 0.2$. This means that a change in the pre-exponential factor from about 1×10^{12} to 1.7×10^{13} s^{-1}, due to the collapsing H_2O structure in going from $\chi_{H_2O} = 0.6$ to $\chi_{H_2O} = 0.0$, may fully account for the observed decrease in triplet lifetime.

4.3.5. The triplet state of 3-nitroanisole

For 3-NA the temperature dependence of the triplet lifetime has been determined in CH_3CH_2OH and CH_3CN. In contrast with 3,5-DINA a long-lived triplet can be observed in CH_3CN. Apparently the triplet state has already $\pi\pi^*$ character here. From the plots shown in Fig. 38 we derive the parameters given in Table 23. Again we observe a relatively low pre-exponential factor in the hydrogen bonding solvent and a pre-exponential factor near the theoretical value in the non-associating CH_3CN. The activation energies in this case probably reflect not only the stabilization due to hydrogen bonding or dipole–dipole interactions of the charge transfer state but also the energy separation between the $^3n\pi^*$ and $^3\pi\pi^*$ state.

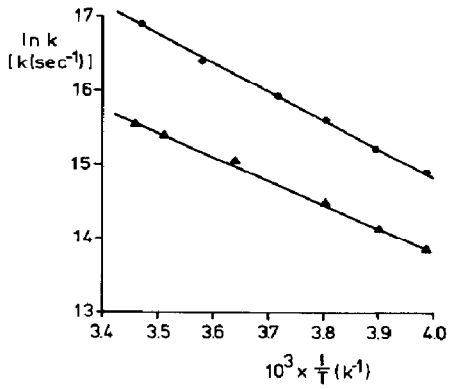

Fig. 38. Arrhenius behaviour of the inverse of the triplet lifetime of 3-NA in CH_3CN (●) and in CH_3CH_2OH (▲).

4.3.6. Mathematical treatment of the kinetics for the decay of $T_{0,HB}$

The concentration of triplet states T_0 as a function of time is given by $a(t)$, and of $T_{0,HB}$ by $b(t)$. The differential equations describing the kinetic scheme in Fig. 32(a) are

TABLE 23
Arrhenius parameters for the inverse of the triplet lifetime of 3-nitroanisole

Solvent	A (s^{-1})	E_a (kJ mol^{-1})
CH_3CN	4.3×10^{11}	28.6
CH_3CH_2OH	1.6×10^{13}	31.5

$$\frac{da(t)}{dt} = -(k_1 + k_3)a(t) + k_2 b(t) \tag{47}$$

with $a(0) = 0$ and

$$\frac{db(t)}{dt} = k_1 a(t) - (k_2 + k_4)b(t) \tag{48}$$

with $b(0) = C_0$. A Laplace transformation of eqns. (47) and (48) yields

$$A(s) = \frac{k_2 C_0}{k_1 k_2 - (s + k_1 + k_3)(s + k_2 + k_4)} \tag{49}$$

$$B(s) = \frac{(s + k_1 + k_3)A(s)}{k_2} \tag{50}$$

The back transformation of eqns. (49) and (50) then yields

$$a(t) = \frac{C_0 k_2}{\gamma_2 - \gamma_1}\{\exp(-\gamma_1 t) - \exp(-\gamma_2 t)\} \tag{51}$$

$$b(t) = \frac{C_0}{\gamma_2 - \gamma_1}\{(k_1 + k_3 - \gamma_1)\exp(-\gamma_1 t) - (k_1 + k_3 - \gamma_2)\exp(-\gamma_2 t)\} \tag{52}$$

Here

$$\gamma_1 = \frac{1}{2}(k_1 + k_2 + k_3 + k_4) - \{(k_1 + k_2 + k_3 + k_4)^2 - 4(k_1 k_4 + k_2 k_3 + k_3 k_4)\}^{1/2} \tag{53}$$

$$\gamma_2 = \frac{1}{2}(k_1 + k_2 + k_3 + k_4) + \{(k_1 + k_2 + k_3 + k_4)^2 - 4(k_1 k_4 + k_2 k_3 + k_3 k_4)\}^{1/2}$$

With substitution of the actual values of the rate constants in eqn. (53) it follows that $\gamma_1 \gg \gamma_2$ and thus

$a(t) \approx 0$

$b(t) \approx C_0 \exp(-\gamma_2 t)$

4.3.7. The theory used to interpret the temperature dependence of the decay rate constant

The empirical expression for the temperature dependence of a reaction rate constant is given by the Arrhenius equation

$$k = A \exp\left(-\frac{E_a}{RT}\right) \tag{54}$$

According to the transition state theory the reaction rate constant can be expressed as

$$k = \frac{k_B T}{h} K^{\ddagger}$$

$$= \frac{k_B T}{h} \exp\left\{-\frac{(\Delta G^\circ)^{\ddagger}}{RT}\right\} \tag{55}$$

or

$$k = \frac{k_B T}{h} \exp\left\{\frac{(\Delta S^\circ)^{\ddagger}}{R}\right\} \exp\left\{-\frac{(\Delta H^\circ)^{\ddagger}}{RT}\right\} \tag{56}$$

in which k_B represents the Boltzmann constant, h is Planck's constant and $K^{\ddagger}$ is the equilibrium constant of the reactants and the transition state. $(\Delta G^\circ)^{\ddagger}$ is the standard free activation energy and $(\Delta S^\circ)^{\ddagger}$ and $(\Delta H^\circ)^{\ddagger}$ are the standard free activation entropy and enthalpy respectively. From eqns. (1) and (3) it follows that

$$k = \frac{2.73 k_B T}{h} \exp\left\{\frac{(\Delta S^\circ)^{\ddagger}}{R}\right\} \exp\left(-\frac{E_a}{RT}\right) \tag{57}$$

Therefore we can directly derive the standard activation entropy from the pre-exponential factor, namely

$$(\Delta S^\circ)^{\ddagger} = 8.3143(\ln A - 30.4575) \tag{58}$$

4.3.8. Concluding remarks concerning hydrogen bonding and excited state lifetimes

Summarizing, we can say that the dissociation of the hydrogen bond between 3,5-DINA in its lowest triplet state and a solvent molecule is in most cases the rate-determining step in the decay of the triplet state to the ground state. The large variations in the triplet lifetime as a function of temperature and solvent composition can be explained by the variation in the rate of dissociation of the hydrogen bond. The magnitude of the activation energy correlates well with expected hydrogen bond strengths but it also depends on solvent–solvent interactions. The magnitude of the activation entropy seems to be determined mainly by solvent–solvent interactions. Both factors are about of equal importance in the lifetime enhancement of the triplet state of 3,5-DINA in hydrogen bonding solvents. It is expected that the above effects are quite general in determining the stability of excited state complexes and may explain numerous temperature and solvent effects on excited state lifetimes such as those discussed by Huber *et al.* [94], Martin [95], Capellos and Suryanarayanan [96] and Bowen *et al.* [93].

Acknowledgments

The authors wish to thank Dr. C. A. de Lange for measuring the reported photoelectron spectra and Professor Dr. J. H. van der Waals for reading and commenting on the entire first draft of the manuscript. The Foundation for Chemical Research in the Netherlands has supported the investigations with financial aid from The Netherlands Organization for the Advancement of Pure Research.

References

1 R. Grinter, E. Heilbronner, M. Godfrey and J. N. Murrell, *Tetrahedron Lett.*, (1961) 771.
2 H. E. Zimmerman and V. R. Sandel, *J. Am. Chem. Soc., 85* (1963) 915.
3 R. Hurley and A. C. Testa, *J. Am. Chem. Soc., 88* (1966) 4430.
4 R. O. de Jong and E. Havinga, *Recl. Trav. Chim. Pays-Bas, 85* (1966) 275.
5 R. W. Anderson, R. M. Hochstrasser, H. Lutz and G. W. Scott, *Chem. Phys. Lett., 28* (1974) 153.
6 C. A. G. O. Varma, J. J. Tamminga and J. Cornelisse, *J. Chem. Soc., Faraday Trans. II, 78* (1982) 265.
7 J. Cornelisse and E. Havinga, *Chem. Rev., 75* (1975) 353.
8 E. Lippert and J. Kelm, *Helv. Chim. Acta, 61* (1978) 279.
9 T. Förster, *Fluoreszenz Organischer Verbindungen*, Vandenhoeck und Ruprecht, Gottingen, 1951.
10 E. Wicke, *Landolt–Börnstein*, Vols. 1 - 2, Springer, Berlin, 6th edn., 1951, p. 37.
11 C. A. G. O. Varma, F. L. Plantenga, C. A. M. van den Ende, P. H. M. van Zeyl, J. J. Tamminga and J. Cornelisse, *Chem. Phys., 22* (1977) 475.
12 L. H. Luthjens, *Rev. Sci. Instrum., 44* (1973) 1661.
13 L. H. Luthjens and A. M. Schmidt, *Rev. Sci. Instrum., 44* (1973) 567.
14 L. A. McLachlan, *J. Magn. Reson., 26* (1977) 223.
15 M. S. Carpenter, W. M. Easter and T. F. Wood, *J. Org. Chem., 16* (1951) 586.
16 E. Liss and K. Lohmann, *Chem. Ber., 89* (1956) 2546.
17 T. Reverdin, *Org. Synth., 1* (1944) 219.
18 E. Buncel, *Can. J. Chem., 44* (1966) 771.
19 W. G. Herkstroeter and G. S. Hammond, *J. Am. Chem. Soc., 88* (1966) 4769.
20 J. B. Birks, in J. B. Birks (ed.), *Organic Molecular Photophysics*, Vol. I, Wiley, New York, 1973, p. 403.
21 R. Hurley and A. C. Testa, *J. Am. Chem. Soc., 90* (1968) 1949.
22 W. C. Petersen and R. L. Letsinger, *Tetrahedron Lett.*, (1971) 2197.
23 R. M. Hochstrasser, in A. H. Zewail (ed.), *Advances in Laser Chemistry*, Vol. 3, Springer, New York, 1978, p. 98.
24 C. V. Shank, E. P. Ippen and O. Teschke, *Chem. Phys. Lett., 45* (1976) 291.
25 B. Kopainsky and W. Kaiser, *Chem. Phys. Lett., 66* (1979) 39.
26 E. von Goldammer and H. G. Hertz, *J. Chem. Phys., 74* (1970) 3734.
27 M. E. Lessing, *5th Int. School on Quantum Electronics, Erice, 1975.*
28 T. J. Chuang and K. B. Eisenthal, *Chem. Phys. Lett., 11* (1971) 368.
29 R. E. Smalley, L. Wharton and D. H. Levy, *J. Chem. Phys., 63* (1975) 4977.
30 N. Mataga and T. Kubota, *Molecular Interactions and Electronic Spectra*, Dekker, New York, 1970, p. 411.
31 K. A. Muszkat and M. Weinstein, *J. Chem. Soc., Perkin Trans. II*, (1976) 1072.
32 L. R. Mahoney, *Angew. Chem., Int. Edn. Engl., 8* (1969) 547.

33 J. J. Tamminga, C. A. M. van den Ende, J. M. Warman and A. Hummel, *Recl. Trav. Chim. Pays-Bas, 98* (1979) 305.
34 T. J. Chuang, G. W. Hoffmann and K. B. Eisenthal, *Chem. Phys. Lett., 25* (1974) 201.
35 W. L. Faust, L. S. Goldberg, T. R. Royt, J. N. Bradford, R. T. Williams, J. N. Schnur, P. G. Stone and R. G. Weiss, in C. V. Shank, E. P. E. Ippen and S. L. Shapiro (eds.), *Picosecond Phenomena,* Springer, Berlin, 1978, p. 43.
36 T. C. Hall, *J. Chem. Phys., 20* (1952) 1745.
37 W. van Havere, A. T. H. Lenstra and H. J. Geise, *Acta Crystallogr., Sect. B, 38* (1982) 3119.
38 D. P. Döpp, D. Müller, *5th IUPAC Symp. on Photochemistry, 1974.*
39 J. J. Tamminga, *Thesis,* Leiden, 1979.
40 R. Englman, *Non Radiative Decay of Ions and Molecules in Solids,* North-Holland, Amsterdam, 1979.
41 R. Englman and J. Jortner, *Mol. Phys., 18* (1970) 145.
42 S. H. Lin and R. Bersohn, *J. Chem. Phys., 48* (1968) 2732.
43 R. W. Anderson, D. E. Damschen, G. W. Scott and L. D. Talley, *J. Chem. Phys., 71* (1979) 1134.
44 G. R. Fleming, A. E. W. Knight, J. M. Morris, R. J. Robbins and G. W. Robinson, *Chem. Phys. Lett., 51* (1977) 399.
45 H. Othani, T. Kobayashi, D. Suzuki and S. Nagakura, *Bull. Chem. Soc. Jpn., 53* (1974) 43.
46 L. J. Noe, E. O. Degenkolb and P. M. Rentzepis, *J. Chem. Phys., 68* (1978) 4435.
47 V. Sundstrom, P. M. Rentzepis and E. C. Lim, *J. Chem. Phys., 66* (1977) 4287.
48 W. A. Wassam and E. C. Lim, *J. Chem. Phys., 68* (1978) 433.
49 W. Siebrand and M. Z. Zgierski, *Chem. Phys. Lett., 58* (1978) 8.
50 A. P. Penner, W. Siebrand and M. Z. Zgierski, *J. Chem. Phys., 69* (1978) 5496.
51 A. Banerjee and J. Simons, *J. Chem. Phys., 71* (1979) 60.
52 S. Okajima and E. C. Lim, *J. Chem. Phys., 69* (1978) 1929.
53 C. Seliskar, O. Khalil and S. McGlynn, in E. C. Lim (ed.), *Excited States,* Vol. I, Academic Press, London, 1974, p. 231.
54 G. N. Lewis and M. Kasha, *J. Am. Chem. Soc., 66* (1944) 2100.
55 H. Eyring, S. H. Lin and S. M. Lin, *Basic Chemical Kinetics,* Wiley-Interscience, New York, 1980.
56 D. Knittel, H. Raizdadeh, H. P. Lin and S. H. Lin, *J. Chem. Soc., Faraday Trans. II, 73* (1977) 120.
57 F. Zuccarello, S. Millefiori and G. Buemi, *Spectrochim. Acta, Part A, 35* (1979) 223.
58 B. Vidal and J. N. Murrell, *Chem. Phys. Lett., 31* (1975) 46.
59 H. Labhart and G. Wagnière, *Helv. Chim. Acta, 46* (1963) 1314.
60 S. Nagakura, M. Kojima and Y. Maruyama, *J. Mol. Spectrosc., 13* (1964) 174.
61 H. Labhart, *Tetrahedron, Suppl., 19* (1963) 223.
62 B. Tinland, *Theor. Chim. Acta, 13* (1969) 171; *17* (1970) 163.
63 C. Sieiro and J. I. Fernández-Alonso, *Chem. Phys. Lett., 18* (1973) 557.
64 O. S. Khalil, C. J. Seliskar and S. P. McGlynn, *J. Mol. Spectrosc., 70* (1978) 74.
65 G. Bendazzoli, F. Bertinelli, P. Palmieri and C. Talliani, *Chem. Phys., 16* (1976) 319.
66 V. G. Plotnikov and V. M. Komarov, *Spectrosc. Lett., 9* (1976) 265.
67 C. A. G. O. Varma and E. J. J. Groenen, *Recl. Trav. Chim. Pays-Bas, 91* (1972) 296.
68 C. A. G. O. Varma, *Helv. Chim. Acta, 61* (1978) 772.
69 C. A. G. O. Varma, *Thesis,* Leiden, 1971.
70 J. Del-Bene, *J. Am. Chem. Soc., 97* (1975) 5330.
71 J. Del-Bene and H. H. Jaffé, *J. Chem. Phys., 48* (1968) 1807, 4050; *49* (1968) 1221; *50* (1969) 1126.
H. H. Jaffé, *QCPE (Quantum Chemistry Program Exchange),* (1976), no. 305.
72 M. D. Gordon and J. F. Neumer, *J. Phys. Chem., 78* (1974) 1868.
73 R. Rossetti and L. E. Brus, *J. Chem. Phys., 70* (1979) 4730.

74 S. P. McGlynn, T. Azumi and M. Kinoshita, *Molecular Spectroscopy of the Triplet State*, Prentice-Hall, Englewood Cliffs, NJ, 1969.
75 T. Kobayashi and S. Nagakura, *J. Electron Spectrosc. Relat. Phenom., 6* (1975) 421.
76 A. Kivinen, J. Murto and L. Kilpi, *Suom. Kemistil. B, 40* (1967) 301.
77 A. Kivinen and J. Murto, *Suom. Kemistil. B, 40* (1967) 6; *42* (1969) 190.
78 H. Seidel, C. Bayer, J. Fruwert and G. Geiseler, *Z. Phys. Chem. (Leipzig), 259* (1978) 625.
79 W. F. Baitinger, P. von R. Schleyer, T. S. S. R. Murty and L. Robinson, *Tetrahedron, 20* (1964) 1635.
80 E. M. Arnett, *Prog. Phys. Org. Chem., 1* (1963) 223.
81 W. Passchier, *Thesis*, Leiden, 1978.
82 W. A. P. Luck, in F. Franks (ed.), *Water, a Comprehensive Treatise*, Vol. 2, Plenum, New York, 1973, p. 235.
83 R. Ahlrichs, *Chem. Phys. Lett., 34* (1975) 570.
84 G. P. de Gunst, *Thesis*, Leiden, 1971.
85 P. D. Sullivan and J. Bolton, *Adv. Magn. Reson., 4* (1970) 39.
86 J. A. Pople, W. G. Schneider and H. J. Bernstein, *High Resolution NMR*, McGraw-Hill, New York, 1959, Chap. 10.
87 D. Jones and M. C. R. Symons, *Trans. Faraday Soc., 67* (1970) 961.
88 C. J. W. Gutch, W. A. Waters and M. C. R. Symons, *J. Chem. Soc. B*, (1970) 1261.
89 W. E. Griffiths, C. J. W. Gutch, G. F. Longster, J. Myatt and P. F. Todd, *J. Chem. Soc. B*, (1968) 785.
90 L. C. Allen, *J. Am. Chem. Soc., 97* (1975) 6921.
91 J. B. F. N. Engberts, in F. Franks (ed.), *Water, a Comprehensive Treatise*, Vol. 6, Plenum, New York, 1980, p. 139.
92 E. S. Amis and J. F. Hinton, *Solvent Effects on Chemical Phenomena*, Academic Press, New York, 1973, Chap. 4.
93 E. J. Bowen, N. J. Holder and G. B. Woodger, *J. Chem. Soc., 66* (1962) 2491.
94 R. J. Huber, M. Mahaney and J. V. Morris, *Chem. Phys., 16* (1976) 329.
95 M. Martin, *Chem. Phys. Lett., 35* (1975) 105.
96 C. Capellos and K. Suryanarayanan, *Int. J. Chem. Kinet., 8* (1976) 529.